united nations
educational, scientific
and cultural
organization

international atomic
energy agency

the
abdus salam
international centre for theoretical physics

SMR/1328/7

School on the Physics of Equatorial Atmosphere

(24 September - 5 October 2001)

Excitation of Equatorial Waves by Tropical Convection

R. Garcia
(National Center for Atmospheric Research, Boulder)

Excitation of Equatorial Waves by Tropical Convection:

Inferences from Global OLR Observations and Comparison with GCMs

Introduction

Deep convection is a major source of energy input to the tropical atmosphere. In a time-mean sense, convection redistributes heat and drives the Hadley and Walker cells; in addition, the unsteadiness of convection is the major excitation mechanism for transient motions in the tropics. Because convection occurs on spatial scales too small to be resolved in General Circulation Models (GCMs), its effects must be parameterized. That is, a method must be devised that produces an estimate of convective effects (e.g., precipitation rate, rate of latent heat release) in terms of fields resolved by the model (e.g., temperature, wind divergence, water vapor mixing ratio).

The parameterizations of convection is an "art", relying not just on physical considerations, but also on experience an empirical "tuning" of convection codes. In general, convective parameterizations produce reasonable agreement between computed annual or seasonal mean precipitation and observations thereof. On the other hand, the variability of parameterized convection has not received much attention until fairly recently, but it is now clear that:

- Different convective parameterizations produce widely different variability, especially at high frequencies (periods < 5 d).

- Convective variability determines the nature of the vertically propagating wave spectrum produced by GCMs

- Some of the difficulties encountered in the simulation of the tropical wind oscillations can be ascribed to insufficient wave forcing by parameterized convection

This lecture discusses some recent research that addresses these issues by examining:

- The variability of convection in the tropical atmosphere as inferred from satellite observations of the outgoing longwave radiation (OLR) field

- The variability of convection as calculated by parameterizations used in different GCMs

- The impact of different convective parameterizations on the "climate" of the tropical middle atmosphere produced by GCMs

OUTLINE

1. OBSERVATIONS OF TROPICAL CONVECTION
   - The GCI dataset
2. CONVECTION IN GCMs
   - Convective parameterizations
3. WAVE EXCITATION
   - Theoretical formulation
4. COMPARISON of GCMs vs OBSERVATIONS
   - Time series of convection
   - Spectra of response and EP fluxes
5. IMPLICATIONS FOR TROPICAL DYNAMICS
   - SAO and QBO
   - MJO
6. CONCLUSIONS

1. The GCI Dataset

- OBSERVATIONS OF OLR FROM ISCCP
  - processed by Salby et al (1991)
  - spatial resolution: 0.7° long. × 0.35° lat.
  - time resolution: 3 hours
- CONVERSION TO HEATING RATES
  - Ricciardulli and Garcia (2000)
  - OLR $\rightarrow T_{br} \rightarrow$DCH
- DCH IS PROXY FOR Q_{conv} IN TROPICS
  - Horizontal distribution and time dependence
  - No information of vertical profile
  - Vertical profile adopted from observations
  - Tends to overestimate convective variance

ESTIMATING Q′ FROM OLR OBSERVATIONS

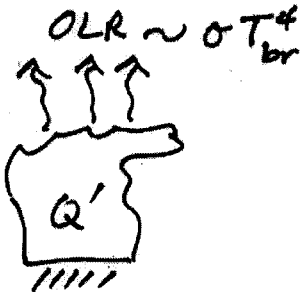

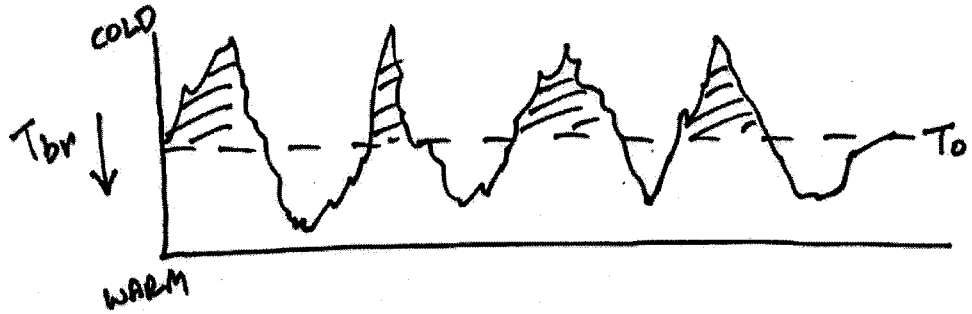

To chosen to emphasize high, cold clouds presumably associated with convection

Deep Convective Activity Index
(Hendon and Woodberry, JGR, 98, 16623 (1993)

$$DCA = \begin{cases} (T_o - T_{br}) & T_{br} < T_o \\ 0 & T_{br} \geq T_o \end{cases}$$

Can be related to precipitation (or latent heat release) by comparing DCA with obs. of precipitation -

$P = a \cdot (T_o - T_{br})$ [Hendon & Woodberry, 1993]

$Q' = b \cdot (T_o - T_{br})$ [Ricciardulli and Garcia, JAS, 57, 3461, 2000]

Estimating Convective Heating from OLR

- Clearly the most desirable way of measuring the effects of convection would utilize a method that observes directly the convective processes in question. For example, tropical precipitation can be measured by a network of raingages or observed by radar. Since precipitation is the result of the condensation of atmospheric water vapor, precipitation rate is directly related to the release of latent heat of condensation. Thus, that reliable observations of the former are also a good indicator of the latter. However, observations of precipitation are often not available on a global basis, so it is necessary to use other, indirect means of estimating precipitation and the attendant latent heat release.

- OLR observations have been made from satellites for many years. The International Satellite Cloud Climatology Project (ISCCP) gathers data from several polar orbiting and geostationary satellites (Schiffer and Rossow, 1983). Some of these data has been reprocessed by M. Salby and colleagues (Tanaka et al., 1991; Salby et al., 1991) into a dataset of OLR covering the entire globe, with horizontal resolution of 0.35° of latitude by 0.7° of longitude, and time resolution of 3 hours. Hendon and Woodberry (1993) have shown how OLR observations can be used to infer convective activity, and this method has been used by Bergman and Salby (1994) and Ricciardulli and Garcia(2000) to estimate global spectra of convective heating.

- OLR methods may overestimate the variance of convection. Recent work by Horinouchi (in press) suggests that overestimation of variance by the OLR method can be severe in some cases. On the other hand, the shape of the spectrum derived from OLR observations is similar to that obtained from redar measurements. See also Ebert et al (1996), and Manton and Ebert (1998).

The following figures show

- Mean and standard deviation of convective heating estimated from OLR observations for winter 1984

- As above, but for the distribution of variance in three frequency bands

- Comparison of spectra of convective precipitation inferred from two OLR methods (dashed curves) and from radar (solid)

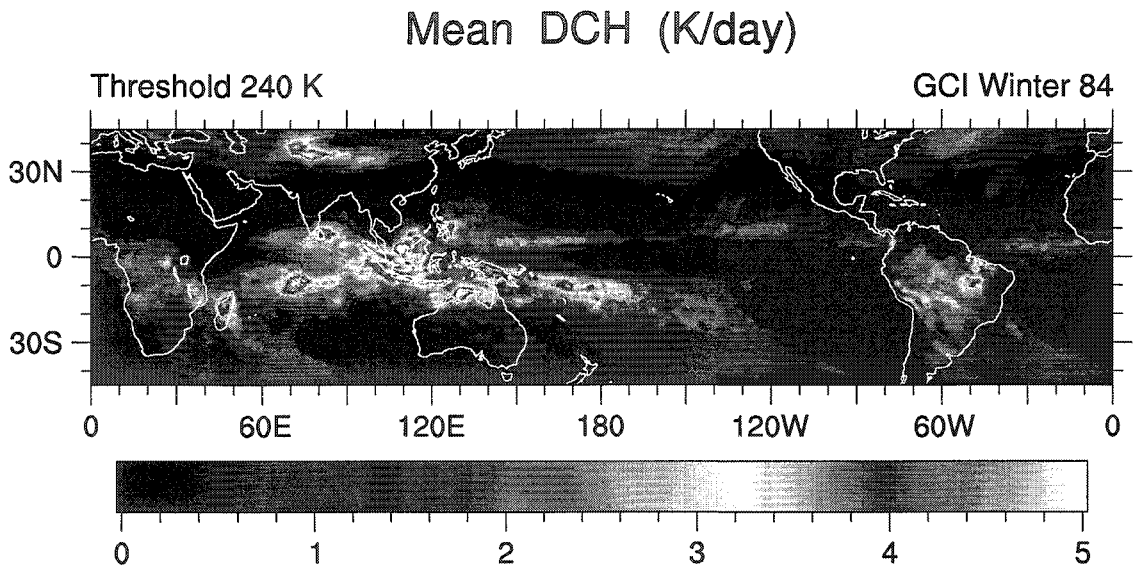
Mean DCH (K/day)
Threshold 240 K
GCI Winter 84
30N
0
30S
0
60E
120E
180
120W
60W
0
0
1
2
3
4
5

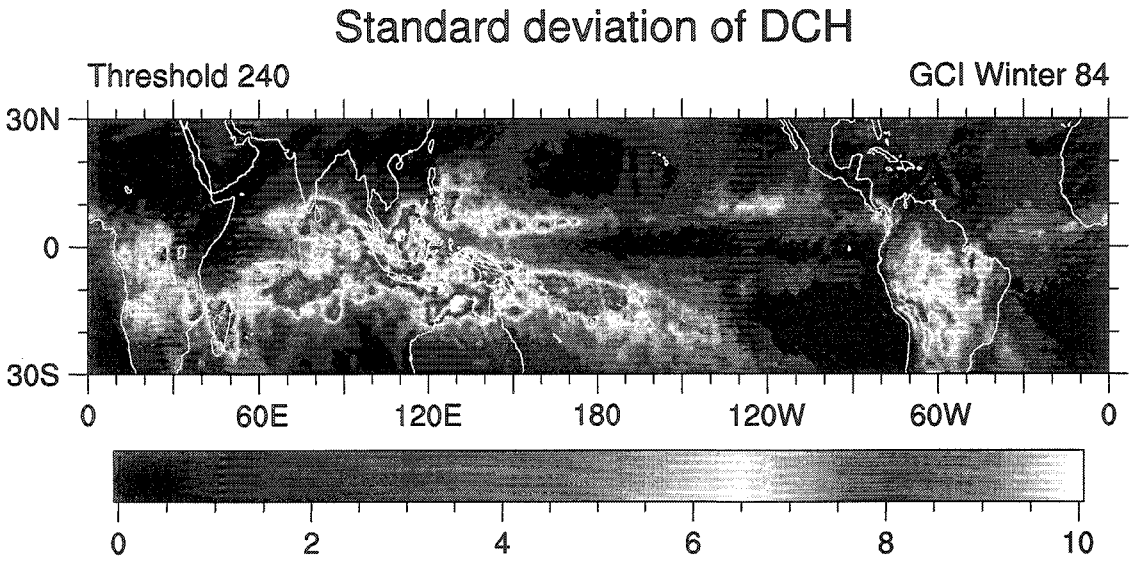
Standard deviation of DCH
Threshold 240
GCI Winter 84
30N
0
30S
0
60E
120E
180
120W
60W
0
0
2
4
6
8
10

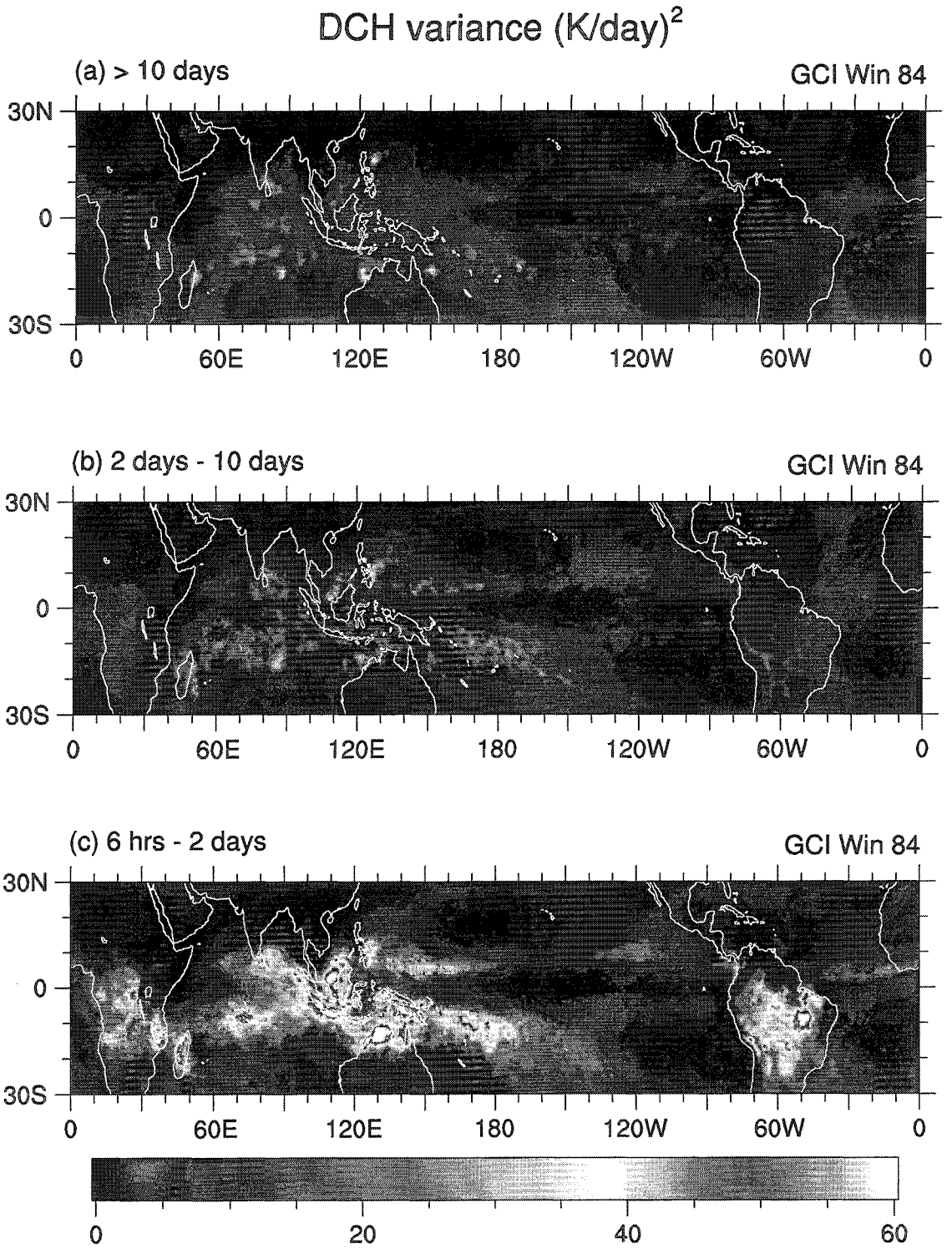
DCH variance (K/day)^2
(a) > 10 days
GCI Win 84
30N
0
30S
0
60E
120E
180
120W
60W
0
(b) 2 days - 10 days
GCI Win 84
30N
0
30S
0
60E
120E
180
120W
60W
0
(c) 6 hrs - 2 days
GCI Win 84
30N
0
30S
0
60E
120E
180
120W
60W
0
0
20
40
60

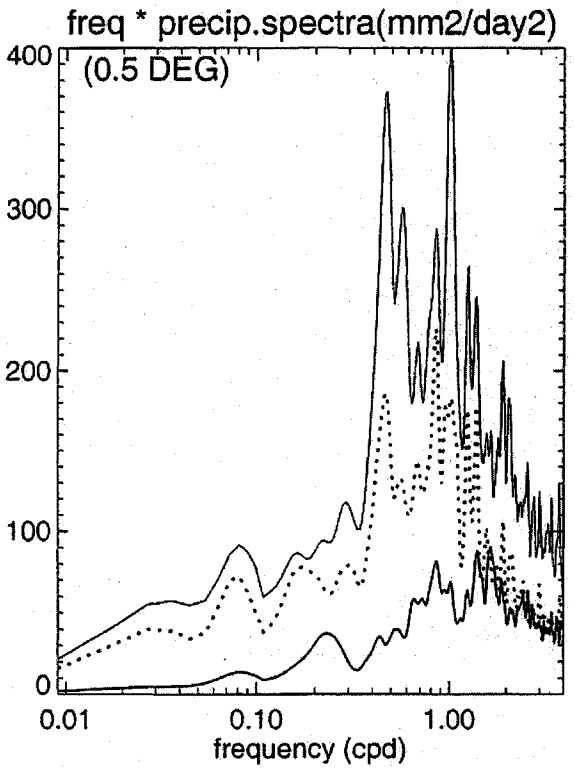
freq * precip.spectra(mm2/day2)
(0.5 DEG)
400
300
200
100
0
0.01
0.10
1.00
frequency (cpd)

2. Convection in GCMs

- Convective processes are small scale (a few km)

- Cannot be resolved in global models

- Parameterizations of convection differ among GCMs
  - NCAR CCM3
    * T42, 30 levels
    * Zhang-McFarlane (1995) parameterization
    * Hack (1984) parameterization
  - Aquaplanet GCM (Horinouchi and Yoden, 1998)
    * T42, 40 levels
    * moist convective adjustment

- All model output of Q_{conv} sampled at 3 hours

Convection statistics are obtained from several state-of-the-art GCMs for analysis and comparison to the estimates from OLR observations. Several examples are shown in the following figures:

- Mean and standard deviation of convective heating in CCM3 with the Zhang-McFarlane convective parameterization
- As above, but for the distribution of variance in three frequency bands
- Mean and standard deviation of convective heating in the ECHAM model
- As above, but for the distribution of variance in three frequency bands

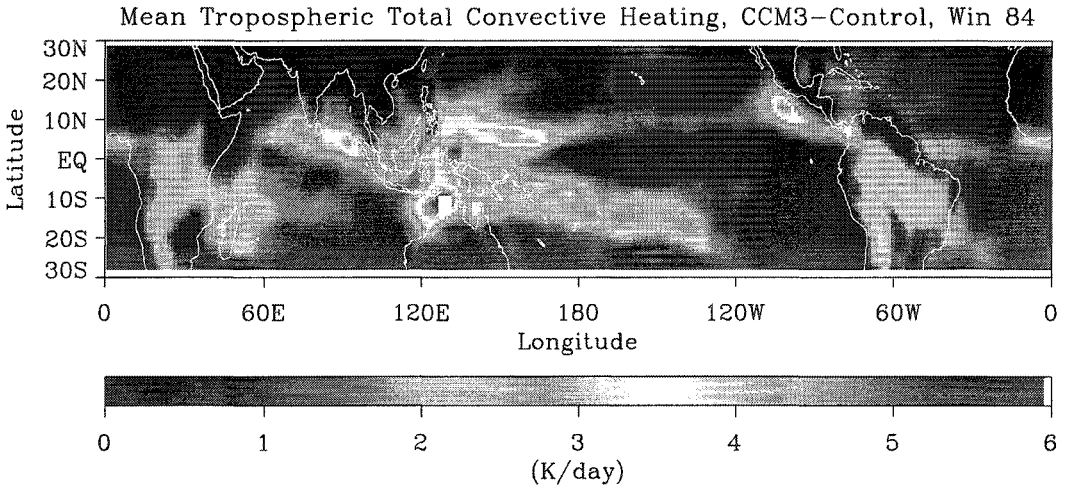
Mean Tropospheric Total Convective Heating, CCM3–Control, Win 84
30N
20N
10N
EQ
10S
20S
30S
Latitude
0
60E
120E
180
120W
60W
0
Longitude
0
1
2
3
4
5
6
(K/day)

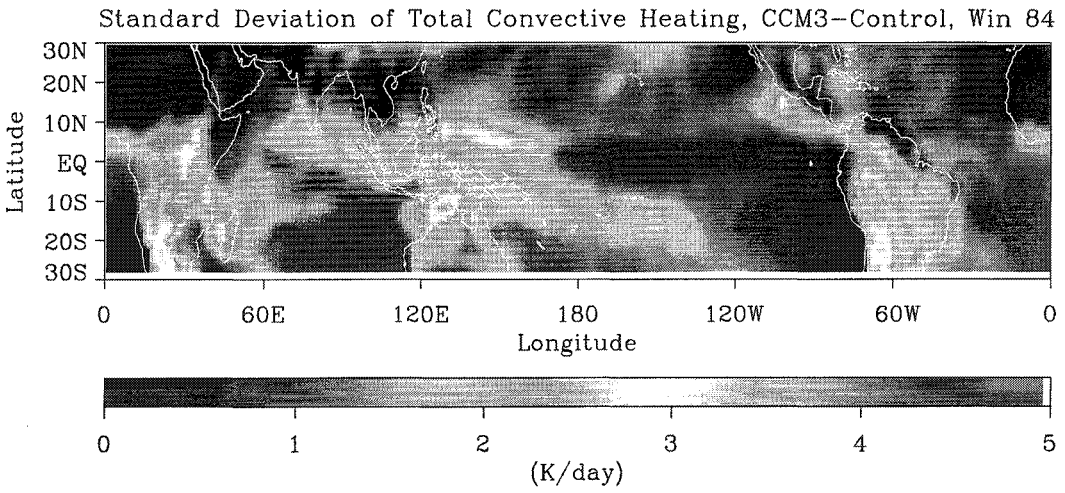
Standard Deviation of Total Convective Heating, CCM3–Control, Win 84
30N
20N
10N
EQ
10S
20S
30S
Latitude
0
60E
120E
180
120W
60W
0
Longitude
0
1
2
3
4
5
(K/day)

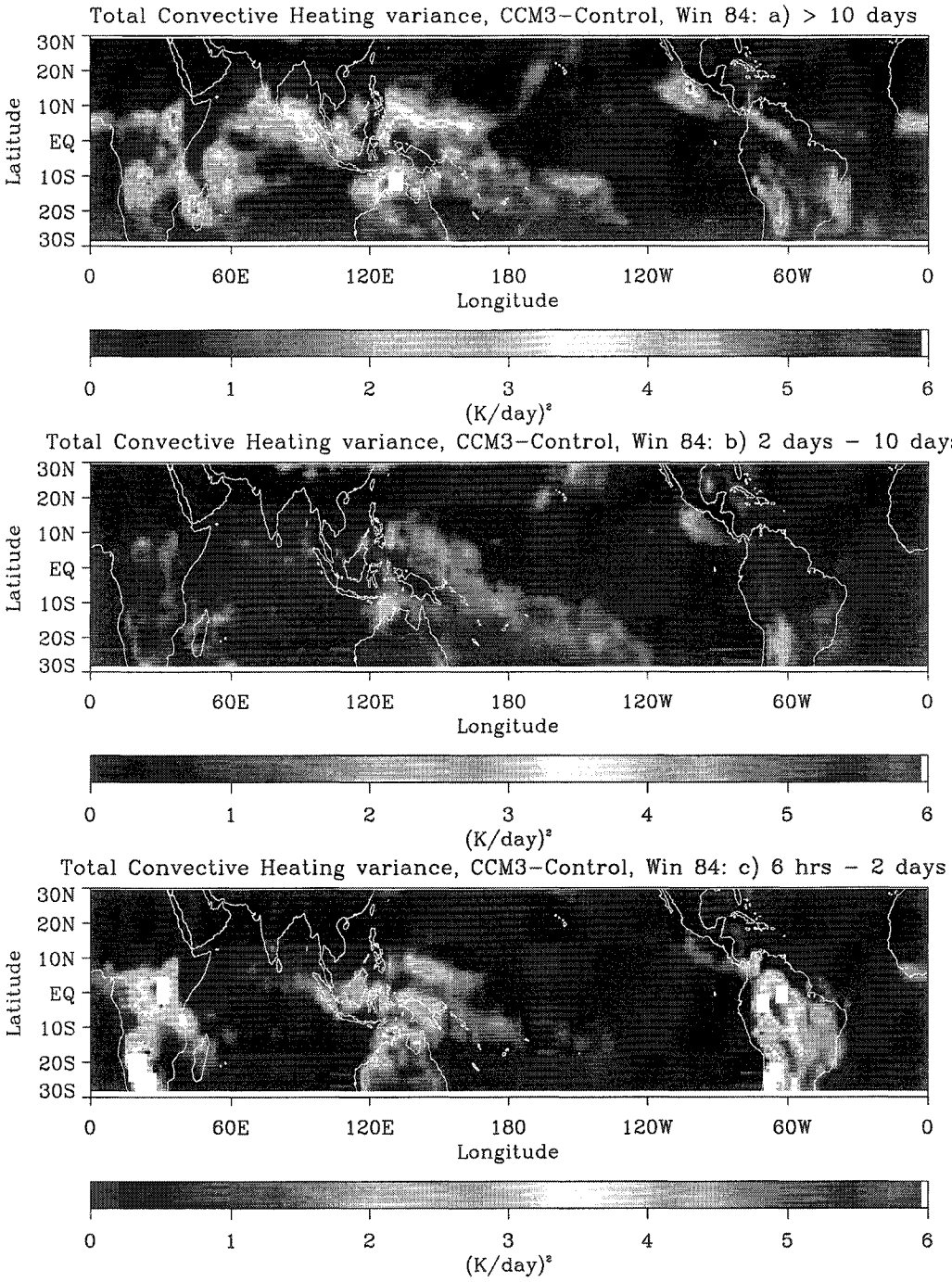
Total Convective Heating variance, CCM3–Control, Win 84: a) > 10 days
30N
20N
10N
EQ
10S
20S
30S
Latitude
0
60E
120E
180
120W
60W
0
Longitude
0
1
2
3
4
5
6
(K/day)²
Total Convective Heating variance, CCM3–Control, Win 84: b) 2 days – 10 days
30N
20N
10N
EQ
10S
20S
30S
Latitude
0
60E
120E
180
120W
60W
0
Longitude
0
1
2
3
4
5
6
(K/day)²
Total Convective Heating variance, CCM3–Control, Win 84: c) 6 hrs – 2 days
30N
20N
10N
EQ
10S
20S
30S
Latitude
0
60E
120E
180
120W
60W
0
Longitude
0
1
2
3
4
5
6
(K/day)²

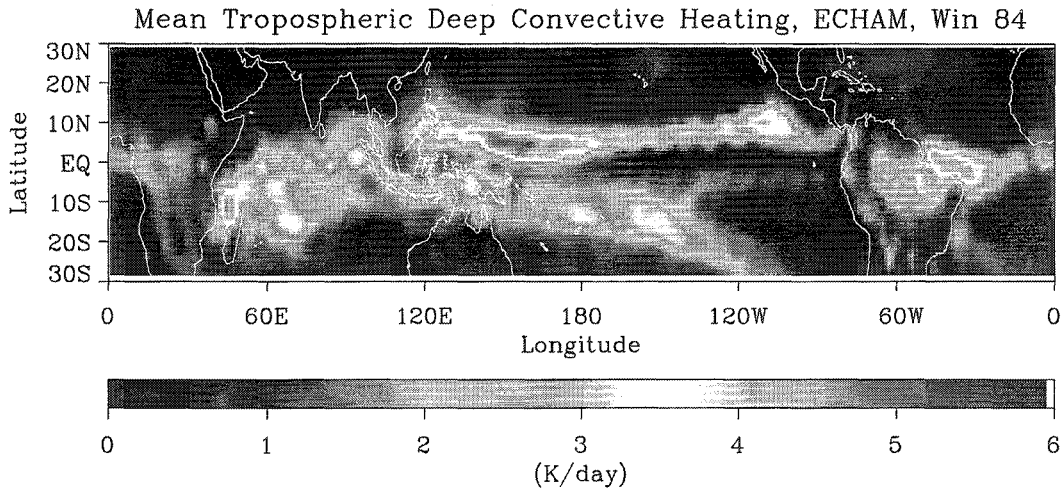
Mean Tropospheric Deep Convective Heating, ECHAM, Win 84
30N
20N
10N
EQ
10S
20S
30S
Latitude
0
60E
120E
180
120W
60W
0
Longitude
0
1
2
3
4
5
6
(K/day)

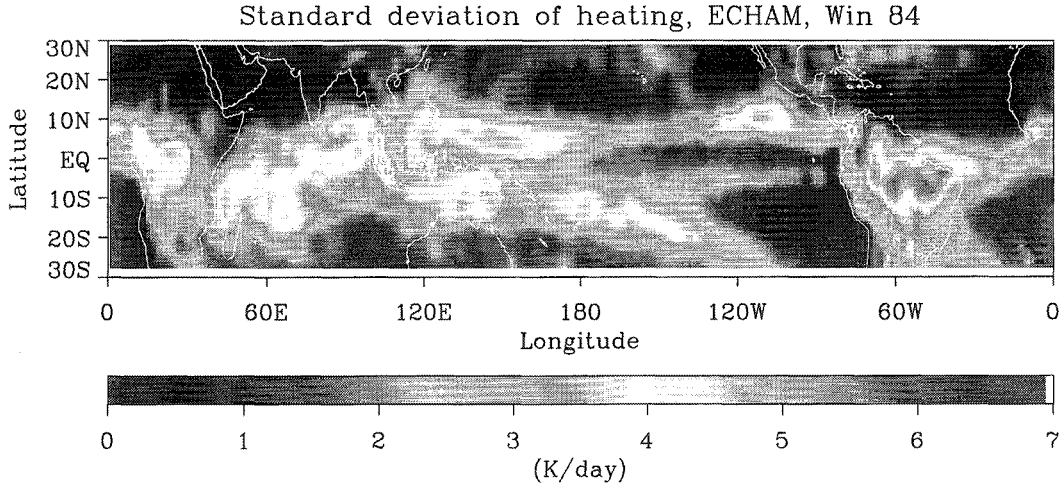
Standard deviation of heating, ECHAM, Win 84
30N
20N
10N
EQ
10S
20S
30S
Latitude
0
60E
120E
180
120W
60W
0
Longitude
0
1
2
3
4
5
6
7
(K/day)

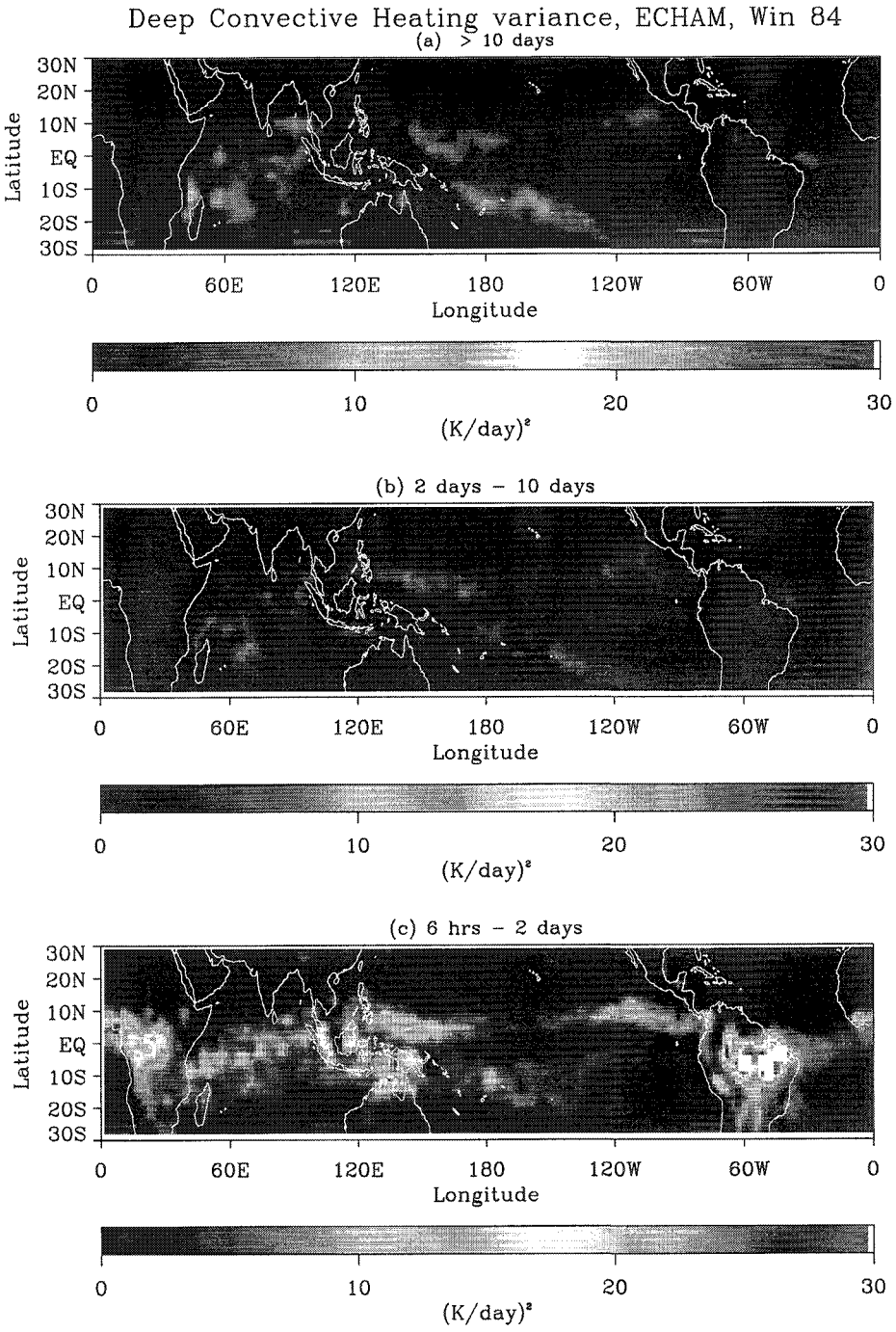
Deep Convective Heating variance, ECHAM, Win 84
(a) > 10 days
30N
20N
10N
EQ
10S
20S
30S
Latitude
0
60E
120E
180
120W
60W
0
Longitude
0
10
20
30
(K/day)²
(b) 2 days – 10 days
30N
20N
10N
EQ
10S
20S
30S
Latitude
0
60E
120E
180
120W
60W
0
Longitude
0
10
20
30
(K/day)²
(c) 6 hrs – 2 days
30N
20N
10N
EQ
10S
20S
30S
Latitude
0
60E
120E
180
120W
60W
0
Longitude
0
10
20
30
(K/day)²

3. Wave Excitation by Convective Heating: Physical Mechanism

$$\left\{\frac{\partial}{\partial t}+\bar{u}\frac{\partial}{\partial x}\right\}T' + w'\frac{HN^2}{R} = Q'_{CONV}$$

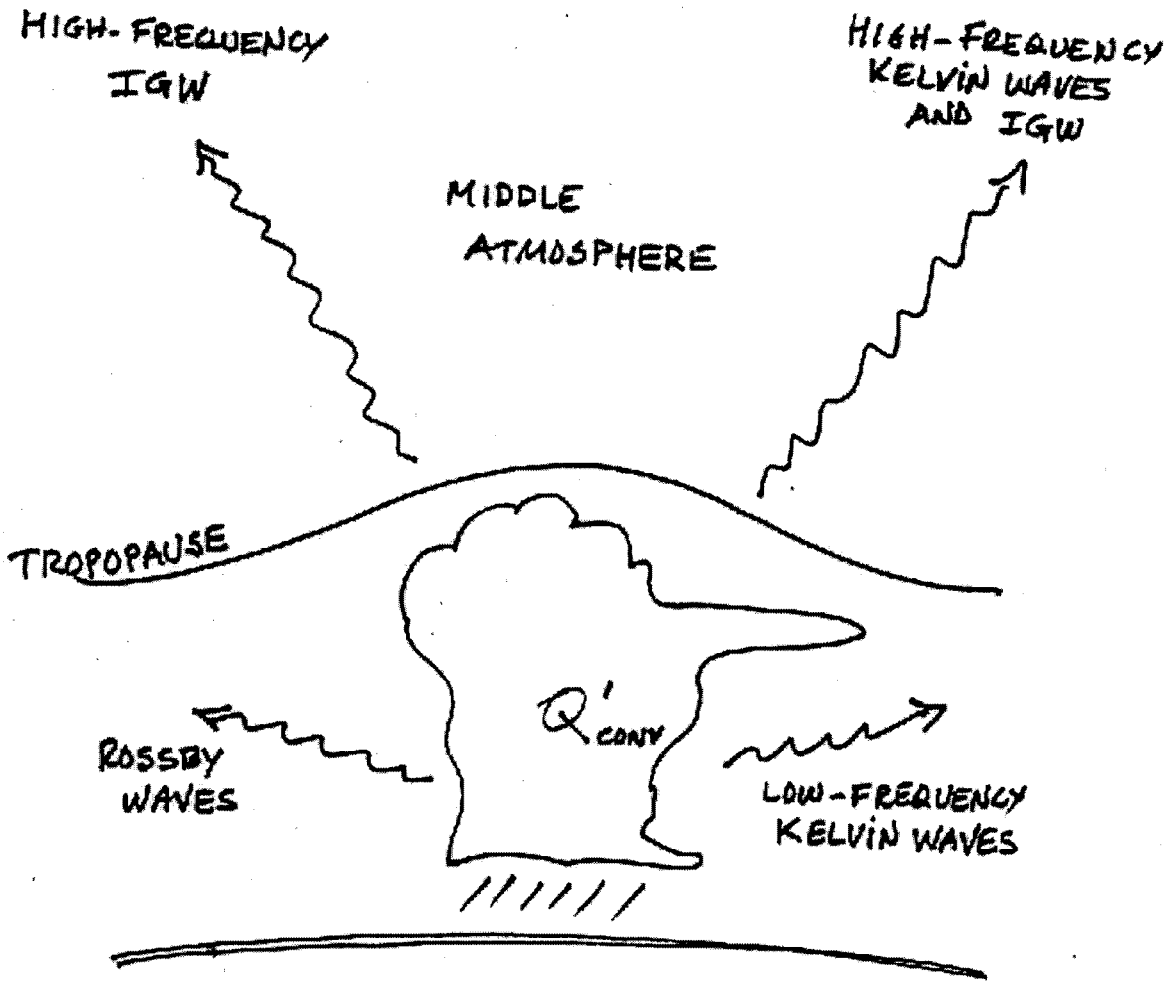

Time-dependent heating can excite equatorial waves when the spatial and temporal characteristics of the heating match those of the waves as determined by their disperison relationship.

- Convective heating enters the governing equations as a time-dependent forcing term in the thermodynamic energy equation (see previous page)

- One can use the method of Salby and Garcia (1987) to obtain estimates of the efficiency with which convective heating excites equatorial waves (as discussed below)

- This depends on frequency, horizontal, and vertical projections of the heating function onto the structure of the various equatorial wave modes

- The vertical projection depends on the depth of the troposphere over which the heating operates; the vertical projection function selects discrete ranges of frequency/wavenumber

Wave Excitation: Theory

Assume:

- Linearized Primitive Equations
- Non Isothermal Atmosphere (N^2 constant)
- Thermal Dissipation α=(10 days)$^{-1}$; no friction
- Decompose all fields into Fourier series in k, ω

Then the governing equation for wave motions is:

$$\mathcal{C}\mathcal{V}[\Phi_k^\omega(\mu,z)] - \mathcal{L}_k^\omega[\Phi_k^\omega(\mu,z)] = \frac{i\kappa}{\omega_D H} e^{z/H} \frac{\partial}{\partial z}\left[e^{-z/H} J_k^\omega(\mu,z)\right]$$

where $\mathcal{C} = \left(\frac{N}{2\Omega a}\right)^2$

This equation is separable,

$$\Phi_k^\omega(\mu,z) = \Sigma_n \Phi_{km}^\omega(z)\Theta_{km}^\omega(\mu)$$

and

$$J_k^\omega(\mu,z) = \Sigma_n Q_{km}^\omega(z)\Theta_{km}^\omega(\mu)$$

where $\Theta_{km}^\omega(\mu)$ are the Hough modes, which satisfy Laplace's Equation.

The system separates into:

- Laplace's Equation

$$\mathcal{L}_k^{\omega}[\Theta_{kn}^{\omega}(\mu)] + \varepsilon_{kn}^{\omega}\Theta_{kn}^{\omega}(\mu) = 0$$

- Vertical Structure Equation

$$\frac{\partial^2 \hat{\Phi}_{kn}^{\omega}}{\partial z^2} + (m_{kn}^{\omega})^2 = \hat{Q}_{kn}^{\omega}$$

where

$$\hat{\Phi}_{kn}^{\omega}(z) = \Phi_{kn}^{\omega}(z)e^{-z/2H}$$

$$\hat{Q}_{kn}^{\omega} = e^{z/2H}\frac{i\kappa}{\omega_D H\Gamma}\frac{\partial}{\partial z}\left[e^{-z/H}Q_{kn}^{\omega}(z)\right]$$

$$\Gamma = 1 + \frac{i\alpha}{\omega_D}$$

and

$$m_{kn}^{\omega} = sgn(\omega)\left[\frac{\epsilon_{kn}^{\omega}\mathcal{C}}{\Gamma} - \frac{1}{4H^2}\right]^{1/2}$$

is the Dispersion Relation.

Assuming $Q^{\omega}_{kn}(z) = \mathcal{Q}^{\omega}_{kn} f(z)$, the **solution** is:

- Vertical structure of individual components

$$\Phi^{\omega}_{kn} = i \frac{\kappa \mathcal{Q}^{\omega}_{kn}}{\omega_D H \Gamma} P^{-}_{m} e^{(1/2H - im)z}$$

where P^{-}_{m}, is a "vertical projection function", which depends on the integral of the heating profile, $f(z)$, times the Green's functions solutions to the vertical structure equation.

(Recall also that $\mathcal{Q}^{\omega}_{kn}$ depends on the projection of the horizontal structure of the heating onto the n^{th} Hough mode.)

- Summation over all Hough modes

$$\Phi^{\omega}_{k}(\mu, z) = \Sigma_n \Phi^{\omega}_{km}(z) \Theta^{\omega}_{km}(\mu)$$

- Total geopotential field

$$\varphi(\mu, z) = \Sigma_{\omega k} \Phi^{\omega}_{k}(\mu, z) e^{ikx} e^{-i\omega t}$$

- The vertical component of EP flux can be expressed in terms of the geopotential

$$[F_z]^{\omega}_{kn} = -\frac{k}{aN^2} \mathrm{Re}(m) \, |\Phi^{\omega}_{kn}(z)|^2$$

Vertical Projection

- It can be shown (Salby and Garcia, 1987) that P_m^- has several maxima, the first two occurring when:

$$\lambda_z = \frac{2\pi}{m} \simeq 2D \quad \text{(First projection response)}$$

$$\lambda_z = \frac{2\pi}{m} \simeq \frac{2}{3}D \quad \text{(Second projection response)}$$

- In all calculations presented, $D = 10$ km

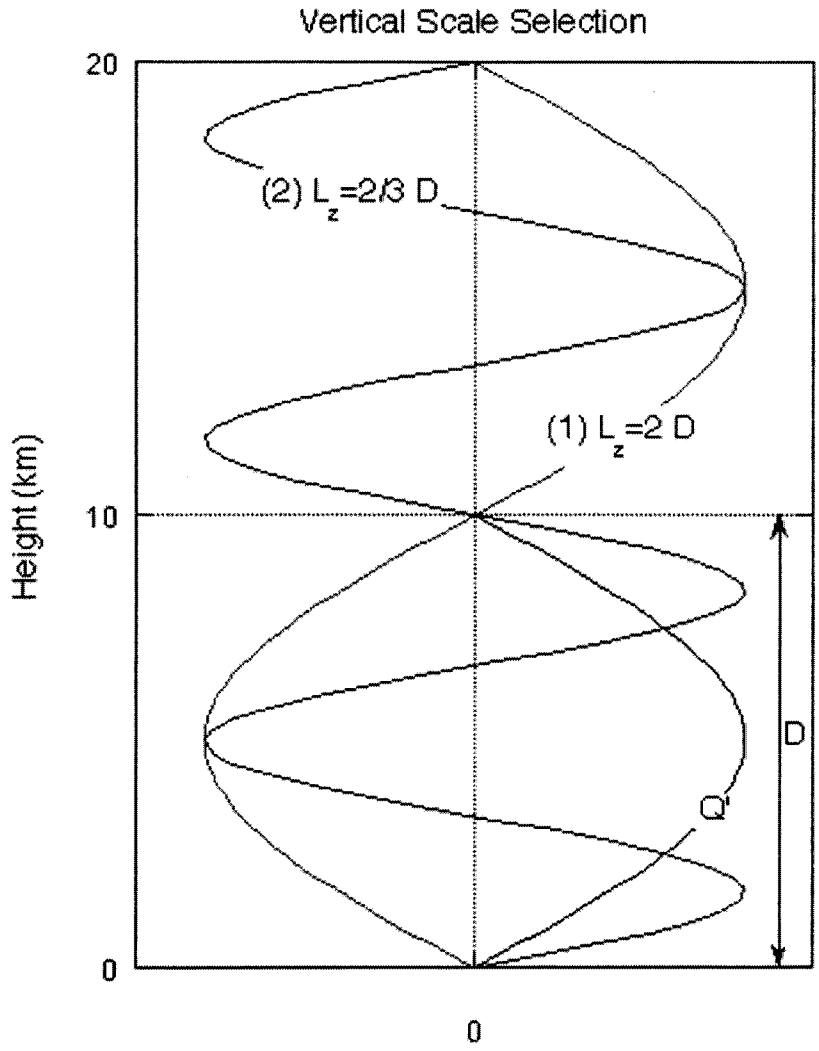
Vertical Scale Selection
20
10
0
Height (km)
(2) L_z=2/3 D
(1) L_z=2 D
D
Q
0

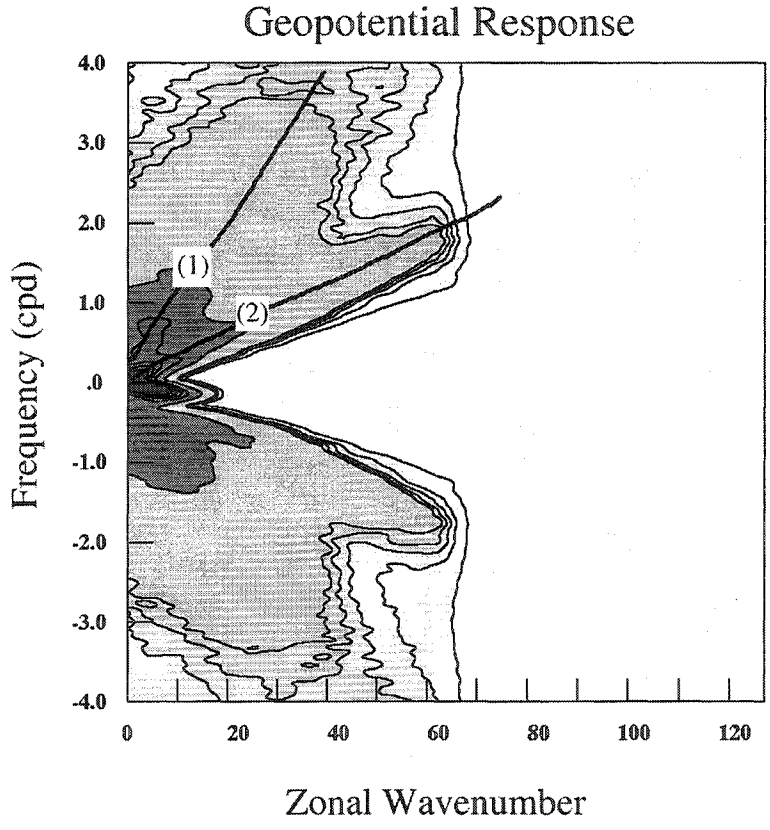
Geopotential Response
4.0
3.0
2.0
1.0
.0
-1.0
-2.0
-3.0
-4.0
Frequency (cpd)
(1)
(2)
0
20
40
60
80
100
120
Zonal Wavenumber

4. Comparisons of GCMs vs Observations

- Time Series at sample gridpoints

- Spectral analyses
  - Spectra of heating
  - Spectra of geopotential
  - Spectral distributions of F_z

The performance of numerical models can be compared with each other and with observations according to several criteria, including:

- Time series of convective heating
- Mean and variance distributions in physical space
- Wavenumber-frequency spectra of heating
- Wavenumber-frequency distributions of vertical component of EP Flux, also inferred from the characteristics of the heating

Comparisons using several of these criteria are shown in the following figures:

- Time series of convective heating at an oceanic location: two NCAR CCM3 runs and OLR data
- Wavenumber-frequency spectra of heating inferred from OLR data compared to spectra obtained with both of the parameterizations used in the NCAR CCM3, and with the parameterization used in AGCM. Some model results resemble the spectrum inferred from OLR data, while some produce relatively little variance at high frequencies
- Wavenumber-frequency spectrum of heating obtained with ECHAM
- Table comparing numerical values of the mean and variance of the heating from the different models
- Spectra as a function of frequency only (summed over all wavenumbers). This figure compares spectra obtained from OLR data with those obtained from the two NCAR CCM3 parameterizations, and from the AGCM

- As above, but comparing OLR, CCM3 running the Zhang-McFarlane parameterization, and ECHAM

- Wavenumber-frequency distribution of the vertical component of EP flux inferred from OLR and obtained with various models.

- As above, for the ECHAM model

- Vertical component of EP Flux as a function of frequency, inferred from OLR observations and calculated from the two NCAR CCM3 parameterizations and from AGCM. The two NCAR models excite inertia-gravity waves weakly

- As above, but comparing OLR with the Hack parameterization in CCM3 and with ECHAM. Note the stronger excitation of inertia-gravity waves

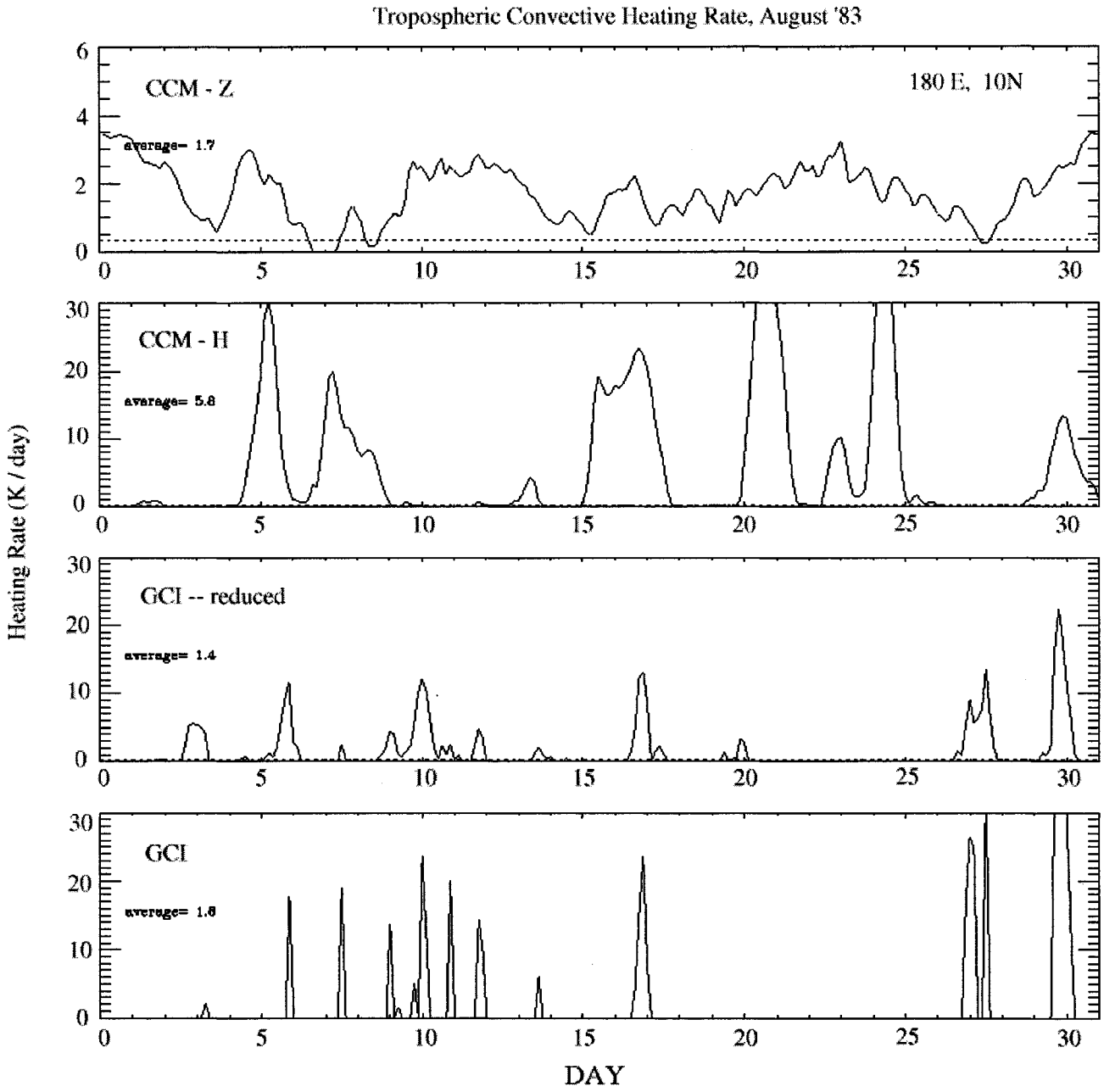
Tropospheric Convective Heating Rate, August '83
CCM - Z
180 E, 10N
average= 1.7
CCM - H
average= 5.8
GCI -- reduced
average= 1.4
GCI
average= 1.6
Heating Rate (K / day)
DAY

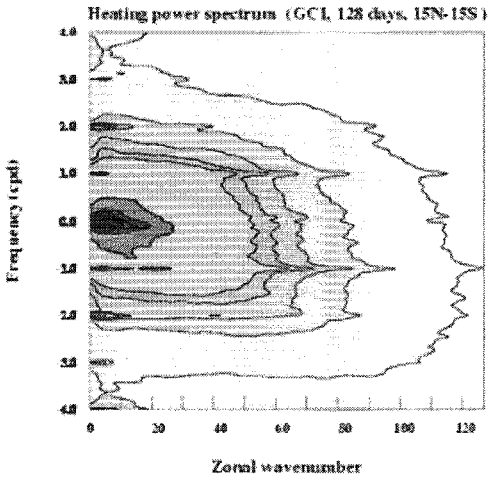
Heating power spectrum (GCI, 128 days, 15N-15S)
Frequency (cpd)
Zonal wavenumber

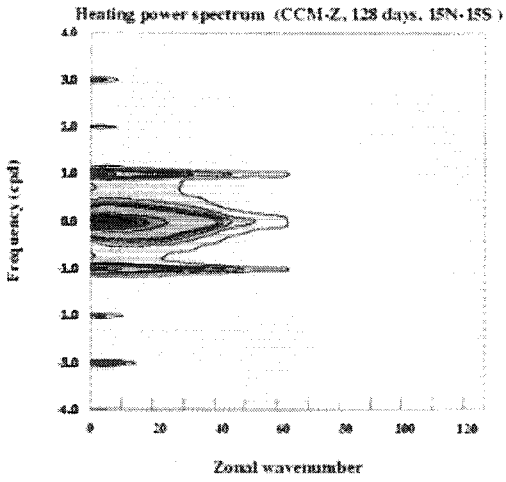
Heating power spectrum (CCM-Z, 128 days, 15N-15S)
Frequency (cpd)
Zonal wavenumber

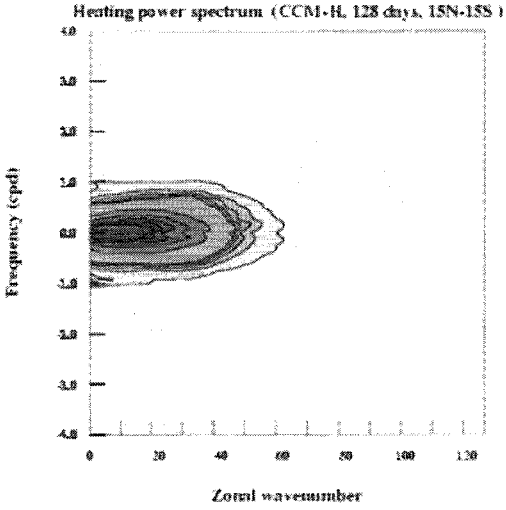
Heating power spectrum (CCM-H, 128 days, 15N-15S)
Frequency (cpd)
Zonal wavenumber

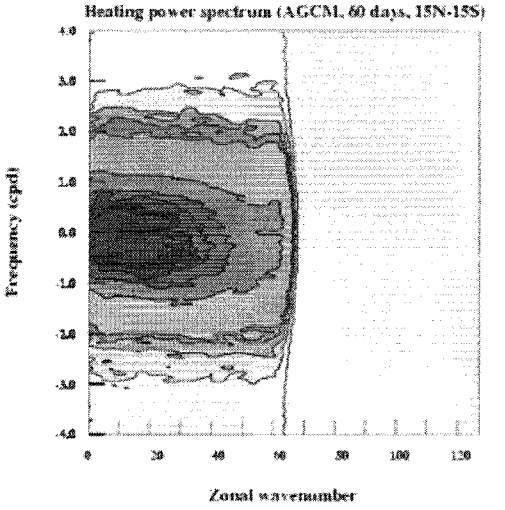
Heating power spectrum (AGCM, 60 days, 15N-15S)
Frequency (cpd)
Zonal wavenumber

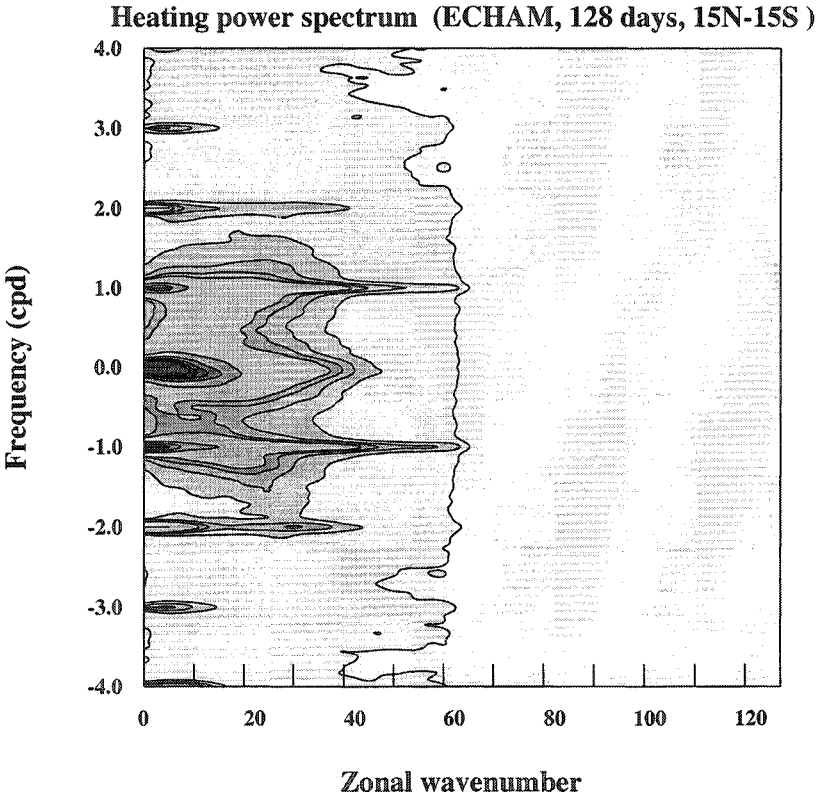
Heating power spectrum (ECHAM, 128 days, 15N-15S)
Frequency (cpd)
4.0
3.0
2.0
1.0
0.0
-1.0
-2.0
-3.0
-4.0
0
20
40
60
80
100
120
Zonal wavenumber

MEAN CONVECTIVE HEATING AND STANDARD DEVIATION (21N–21S) FOR GCI AND VARIOUS GCMs

	GCI	CCMZ	CCMH	AGCM	ECHAM
Mean (K d^{-1})	1.0	1.1	1.1	0.3	1.3
VAR (K^2 d^{-2})					
$\tau > 10$ d	2.2	0.7	5.5	1.1	1.5
$2 < \tau < 10$ d	4.4	0.4	8.3	3.1	1.4
6 hr $< \tau < 2$ d	11.0	0.4	1.5	4.1	4.1
TOTAL (K^2 d^{-2})	17.6	1.5	15.3	8.3	7.0

HEATING POWER SPECTRA COMPARISON, (15N–15S)

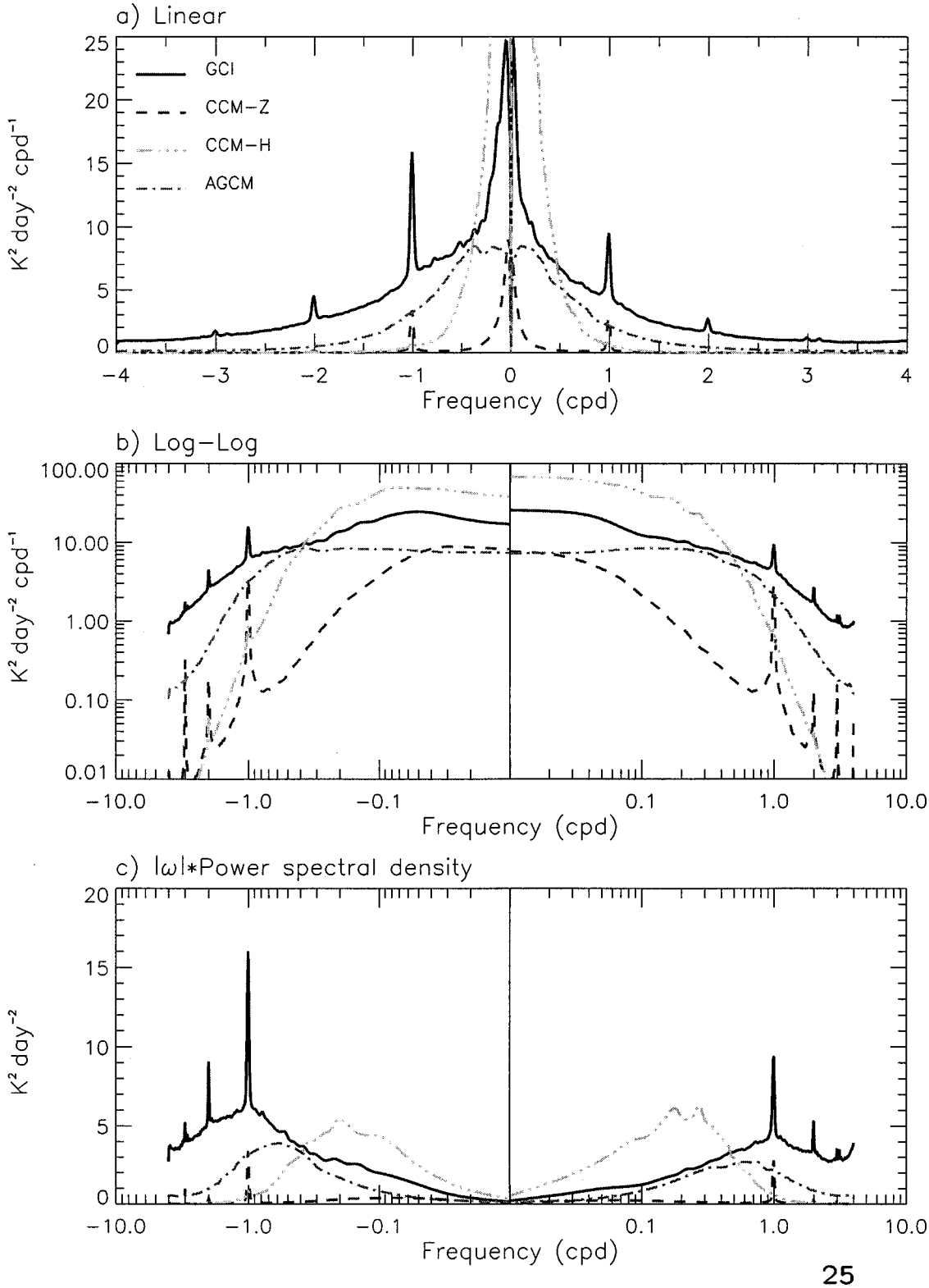

HEATING POWER SPECTRA COMPARISON, (15N–15S)

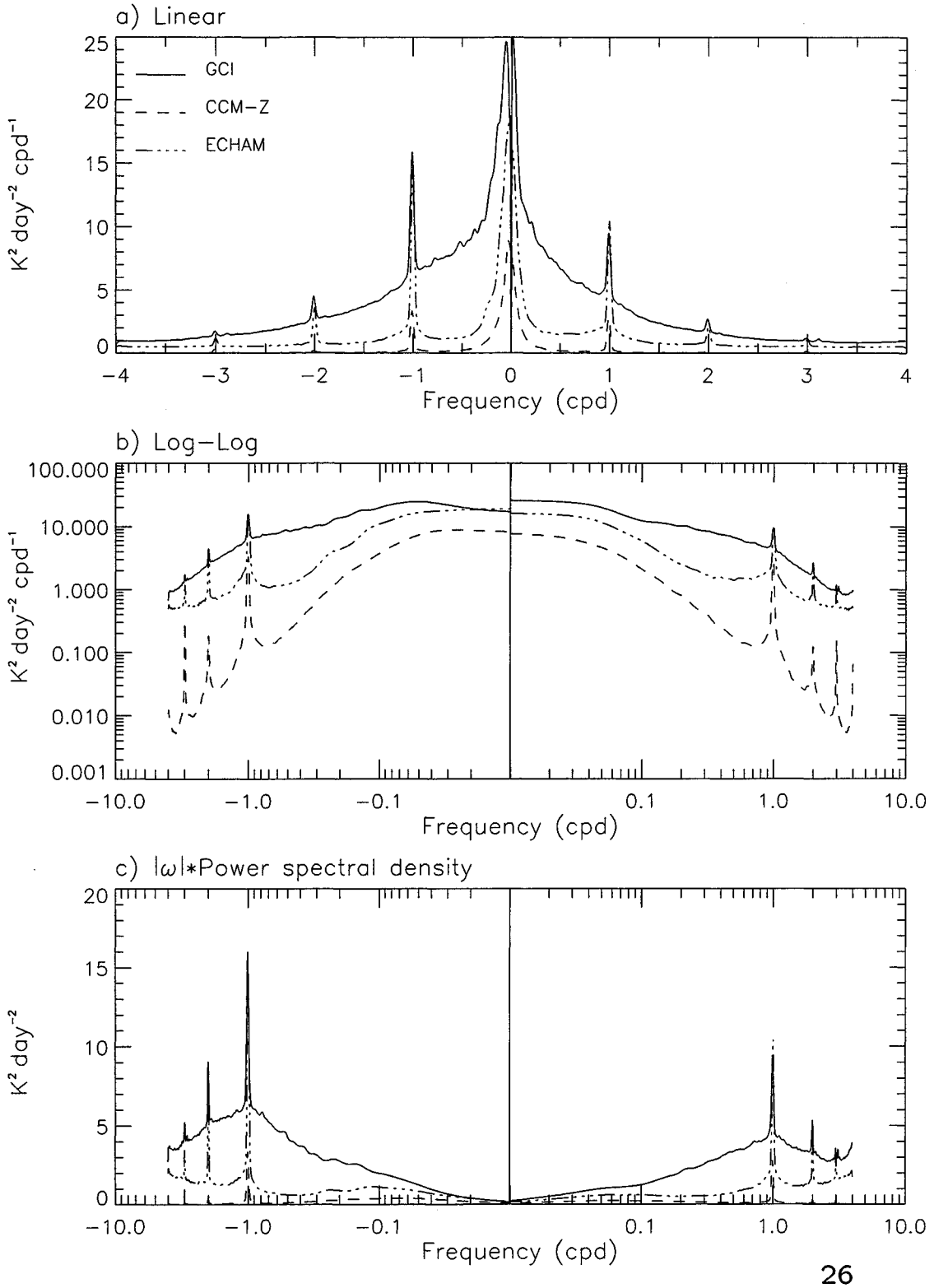

Vertical Component of EP Flux

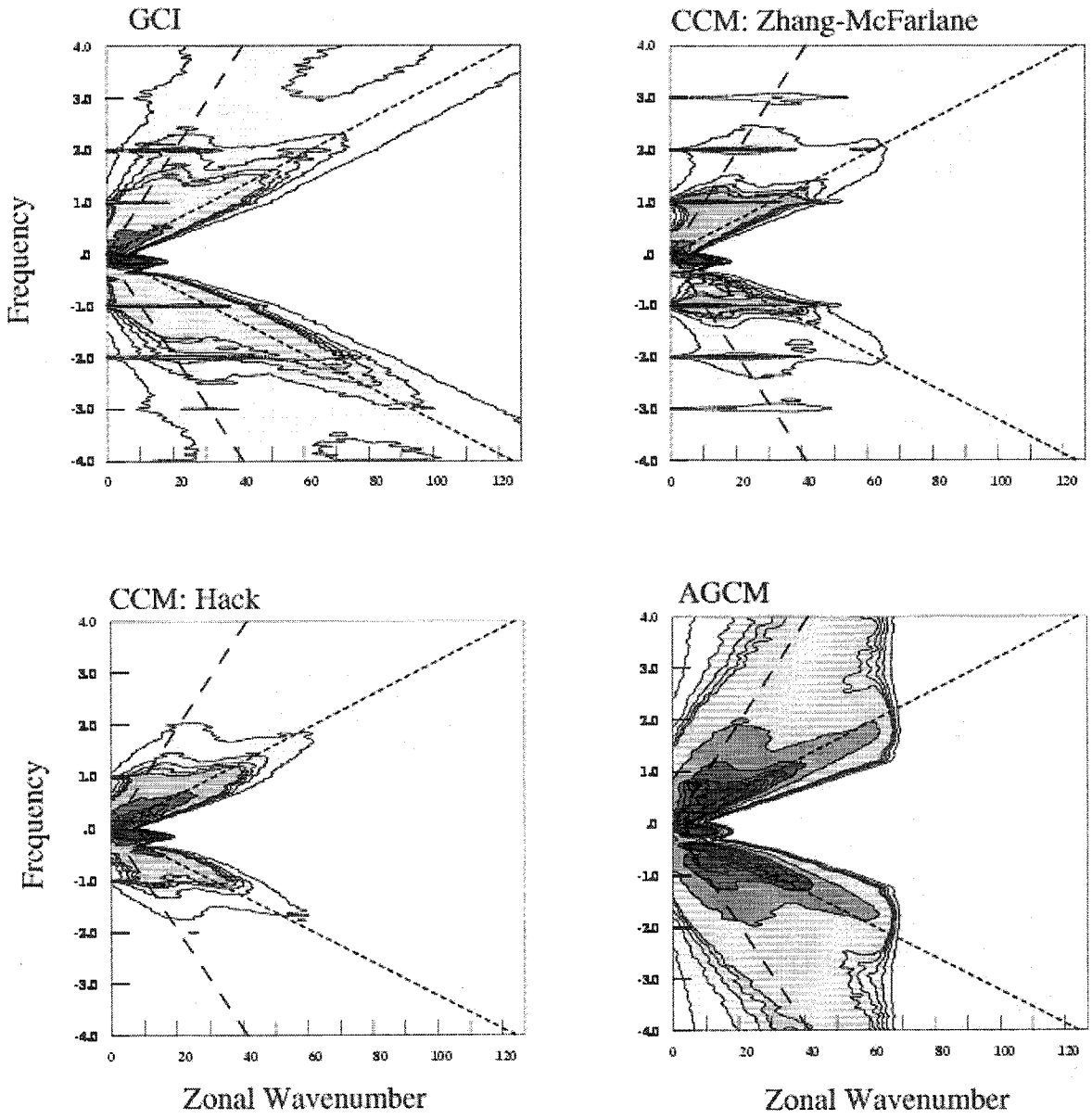

VERTICAL COMPONENT OF EP FLUX COMPARISON

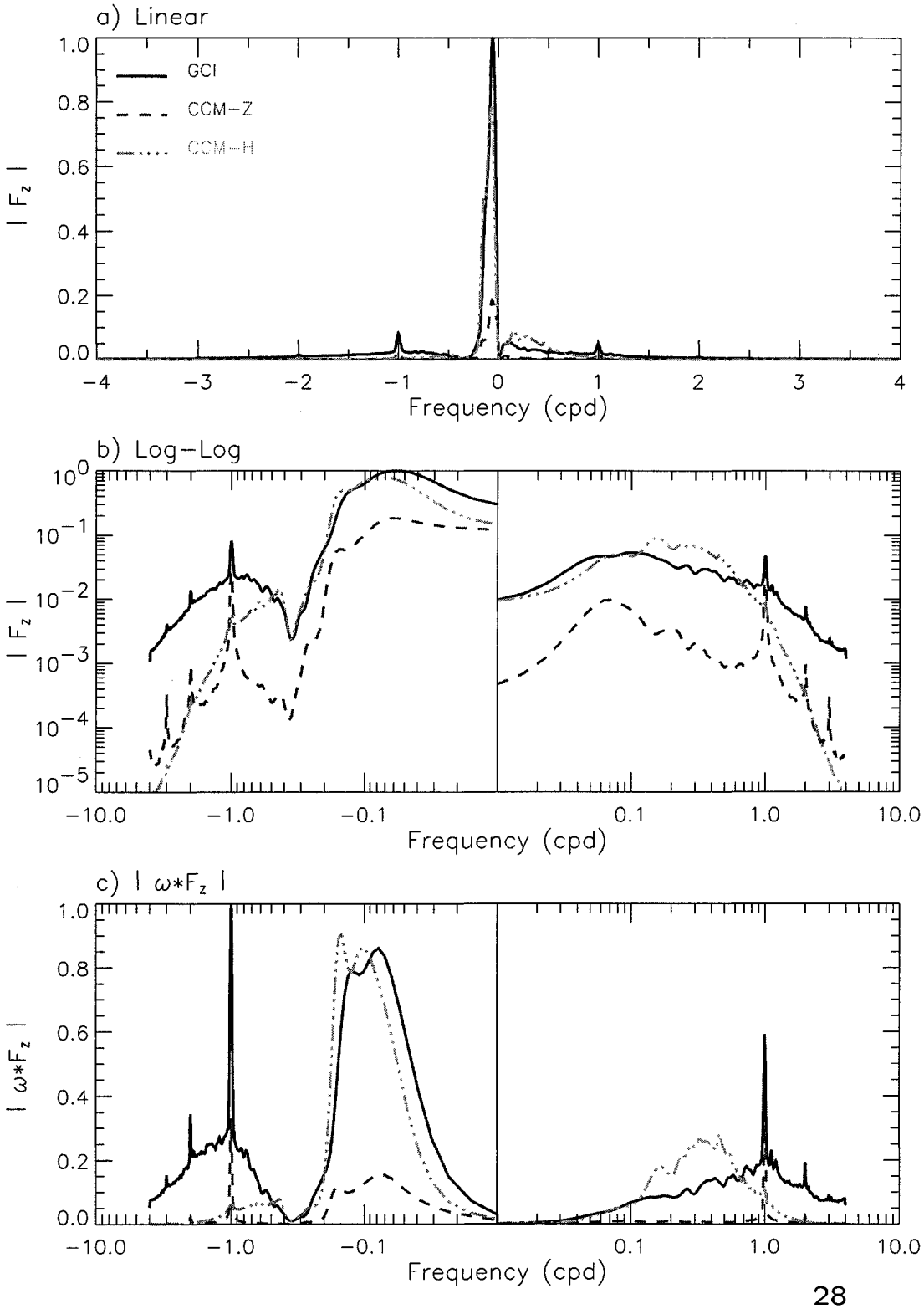

VERTICAL COMPONENT OF EP FLUX COMPARISON

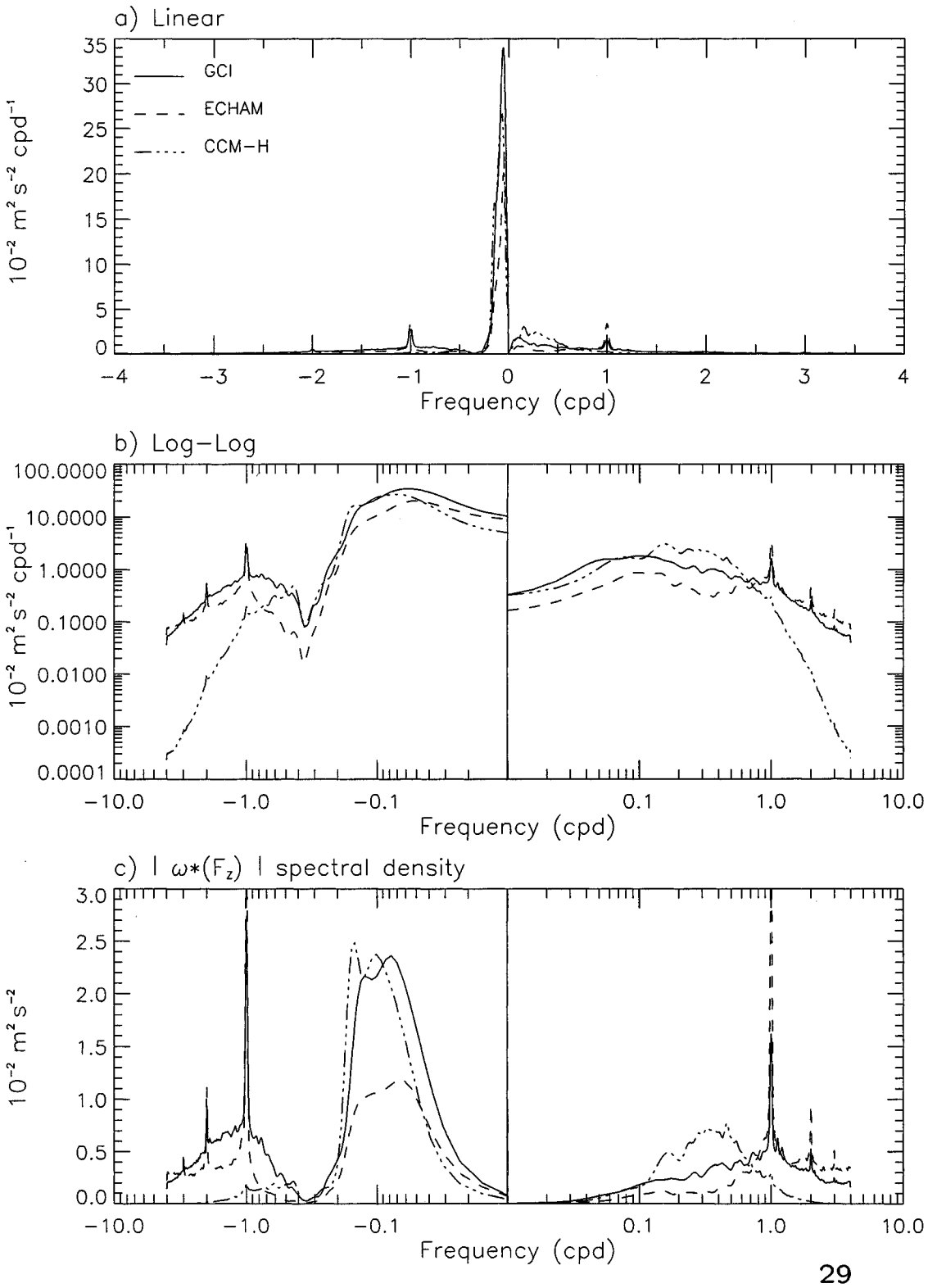

5. IMPLICATIONS FOR TROPICAL DYNAMICS

- Convective parameterizations usually designed to reproduce the mean distribution of convective heating

- Parameterized convective heating often misrepresents actual heating variability

- Convective heating is main excitation mechanism for transient motions in the Tropics

- Vertically-propagating waves
  - QBO and SAO

- Wave phenomena in the troposphere
  - Madden-Julian Oscillation

The SAO and QBO

- Wave driving plays a central role in both wind oscillations

- High phase velocity waves are likely to be most effective for the SAO; lower phase velocity waves, for the QBO

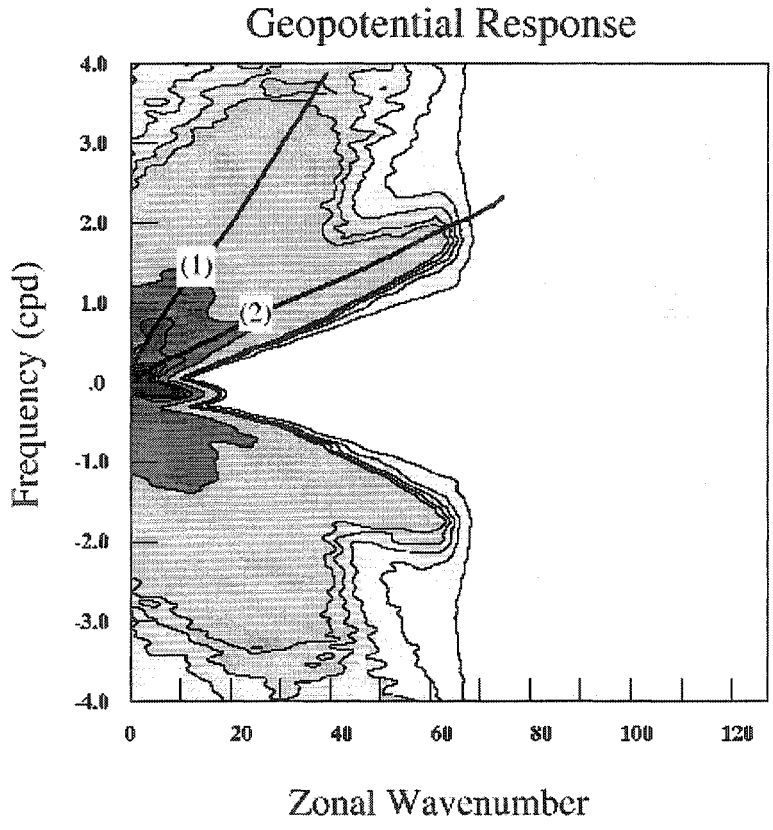

To examine the effect of differences in the spectra of excited waves on the performance of GCMs, consider different ranges of phase velocity. Fast waves are more likely to influence the SAO because they are better able to propagate to high altitudes; slower waves are more likely to be involved in the forcing of the QBO. Accordingly, consider seprately the performance of models for:

- Waves of phase velocity $c > 30$ m s^{-1}.
- Waves of phase velocity $c < 30$ m s^{-1}.

These ranges of c correspond roughly to first and second vertical projection response maxima discussed earlier

Waves of $c > 30$ m s^{-1}

The following figures show:

- Frequency spectra of F_z inferred from OLR data and derived from the NCAR CCM3 using the Hack convective parameterizations. The model produces variance of F_z comparable to that inferred from OLR for Kelvin waves, but underestimates the forcing of inertia-gravity waves. The Zhang-McFarlane parameterization (not shown) underestimates the forcing for all waves and almost all frequencies compared to the OLR results

- The zonal wind at the Equator in three runs of the NCAR CCM3: In the top panel CCM3 is run with the Zhang-McFarlane parameterization *plus* additional forcing due to a specified spectrum of (unresolved) small-scale gravity waves. The middle panel shows a run with the same model except that small-scale gravity wave driving is removed; the SAO disappears in this run. Comparison of these two runs suggests that small-scale gravity wave driving is necessary to simulate the SAO. However, the bottom panel shows a CCM3 run using the Hack convection parameterization and *no* small-scale gravity wave driving. The SAO reappears in this run. One may conclude that (1) there is more than one way to produce a SAO in a GCM; (2) if the frequency distribution of F_z inferred from OLR is correct, then small-scale gravity wave driving may not be essential for producing the SAO.

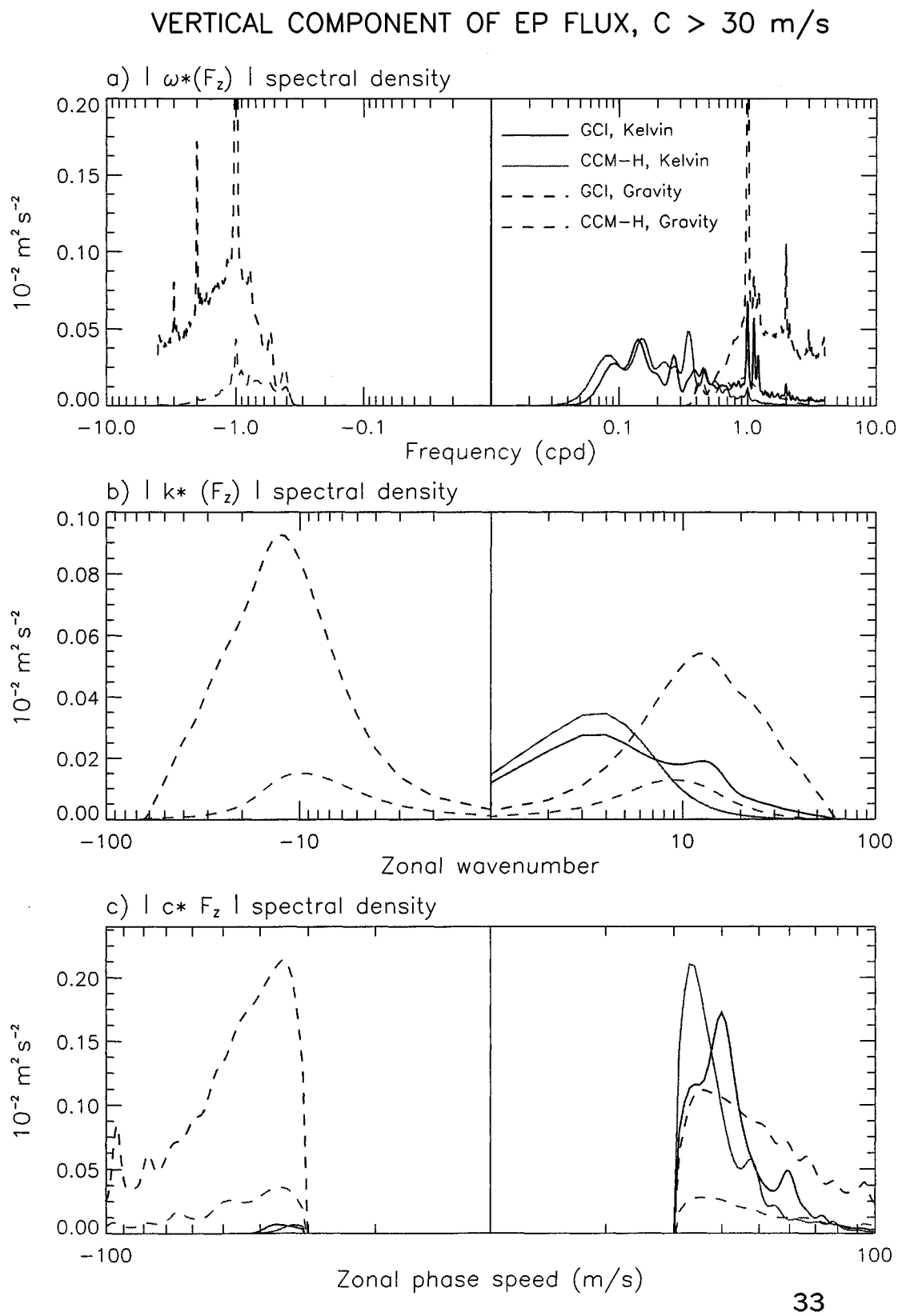
VERTICAL COMPONENT OF EP FLUX, C > 30 m/s
a) | ω*(Fz) | spectral density
GCI, Kelvin
CCM–H, Kelvin
GCI, Gravity
CCM–H, Gravity
0.20
0.15
0.10
0.05
0.00
10⁻² m² s⁻²
–10.0
–1.0
–0.1
0.1
1.0
10.0
Frequency (cpd)
b) | k* (Fz) | spectral density
0.10
0.08
0.06
0.04
0.02
0.00
10⁻² m² s⁻²
–100
–10
10
100
Zonal wavenumber
c) | c* Fz | spectral density
0.20
0.15
0.10
0.05
0.00
10⁻² m² s⁻²
–100
100
Zonal phase speed (m/s)

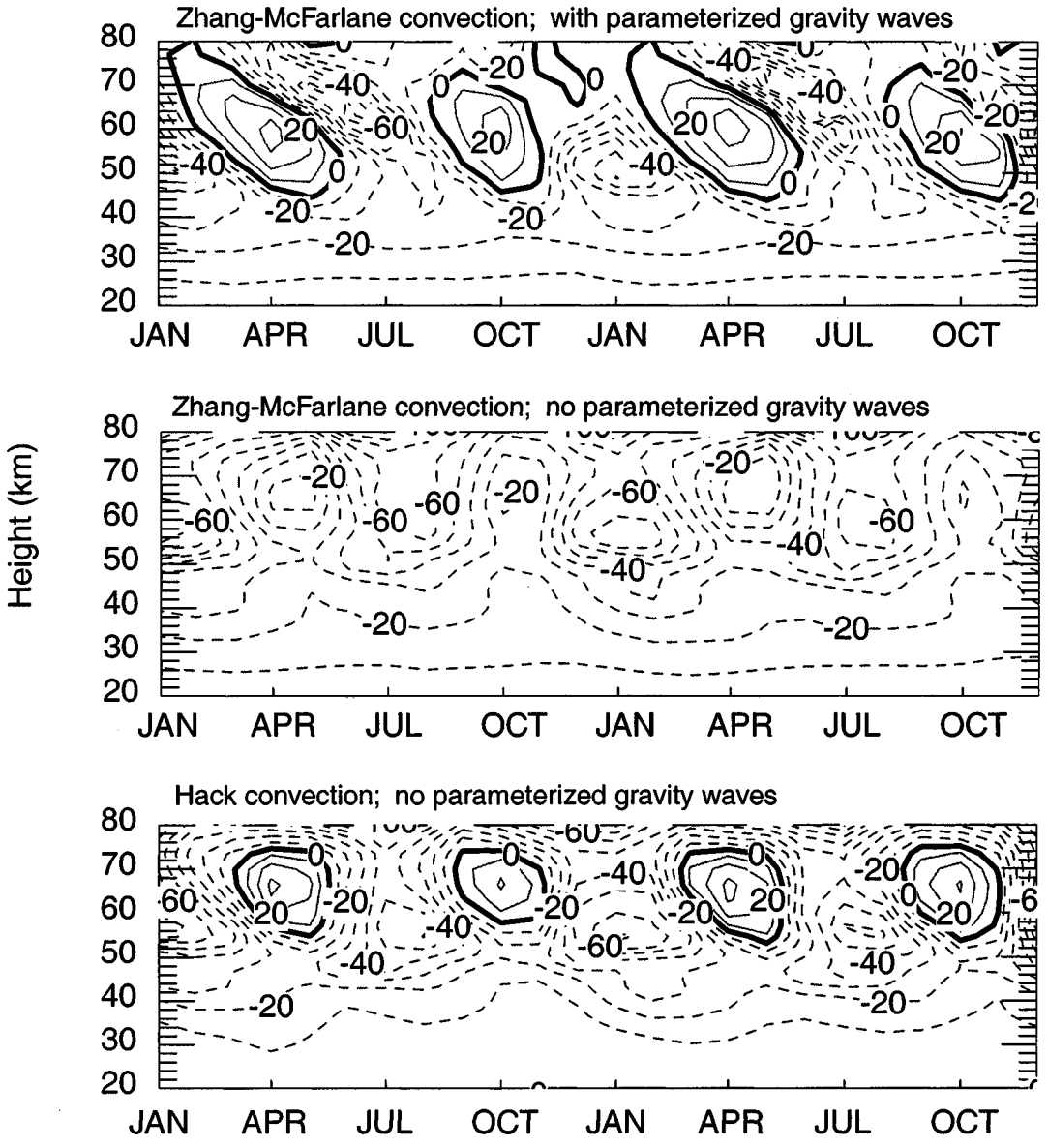
Zhang-McFarlane convection; with parameterized gravity waves
Zhang-McFarlane convection; no parameterized gravity waves
Hack convection; no parameterized gravity waves
Height (km)
80
70
60
50
40
30
20
JAN
APR
JUL
OCT
JAN
APR
JUL
OCT

Waves of $c < 30$ m s^{-1}

The following figures show:

- Frequency spectra of F_z inferred from OLR data and derived from the NCAR CCM3 with the Hack convective parameterizations. Compared to the OLR results, excitation of inertia-gravity waves is weak in the CCM3 run

- Frequency spectra of F_z inferred from OLR data and derived from the AGCM model. Excitation of inertia-gravity waves is comaparable for the model and the OLR observations in this case

- Zonal wind evolution inthe equatorial lower stratosphere in the AGCM. A QBO is evident in the lower stratosphere (sigma coordinate = 0.1 corresponds to 100 mb)

VERTICAL COMPONENT OF EP FLUX, C < 30 m/s

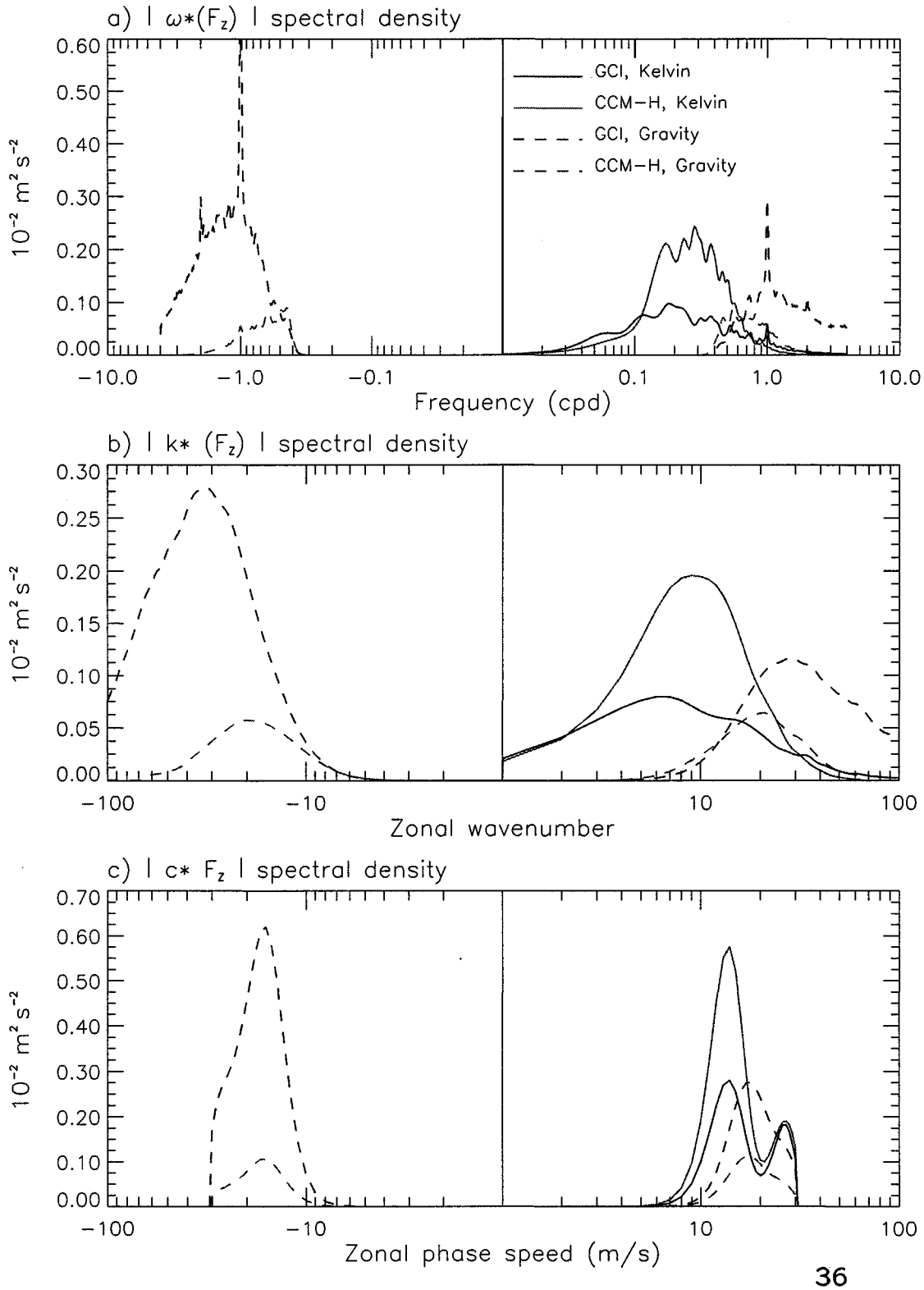

VERTICAL COMPONENT OF EP FLUX, C < 30 m/s

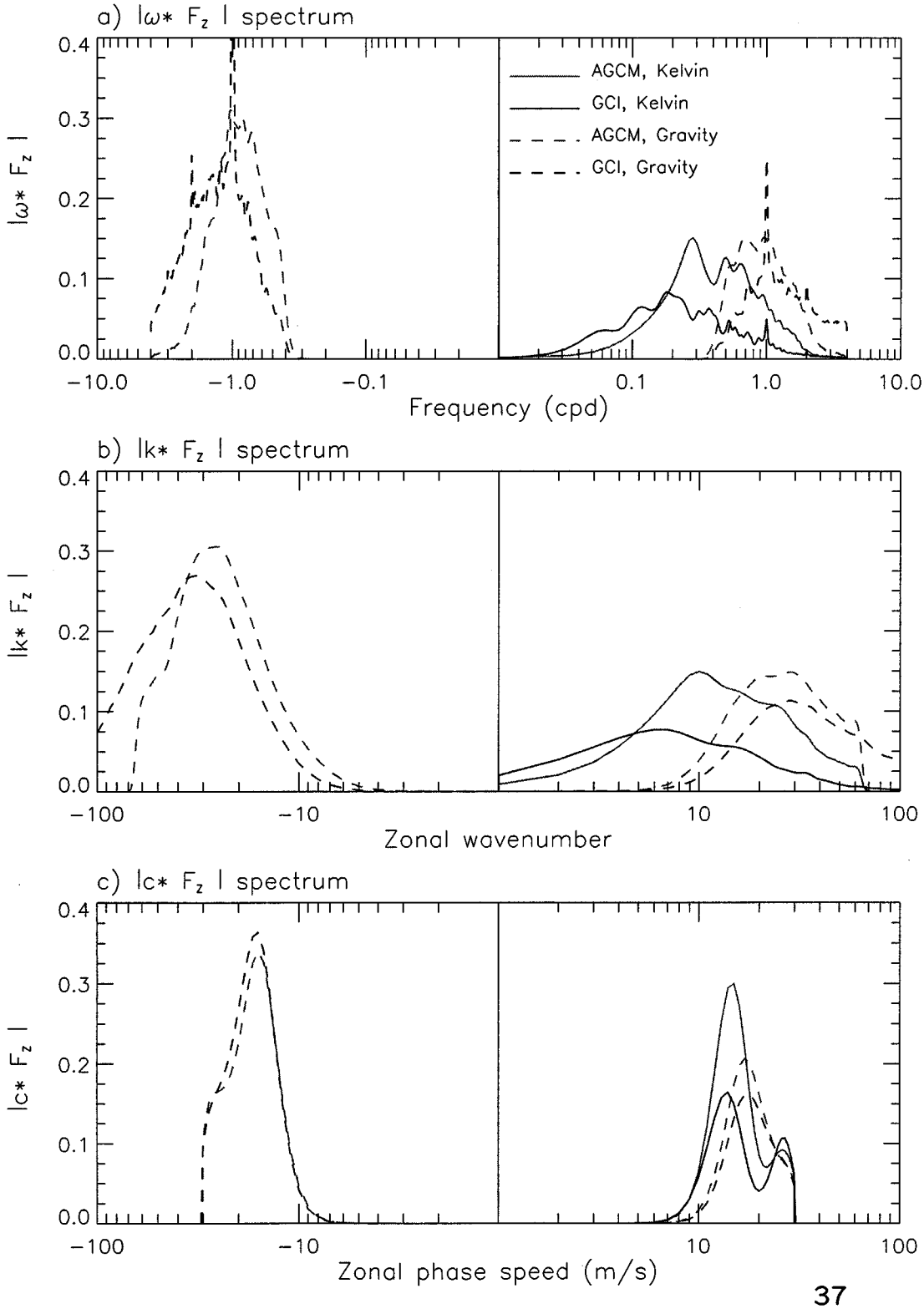

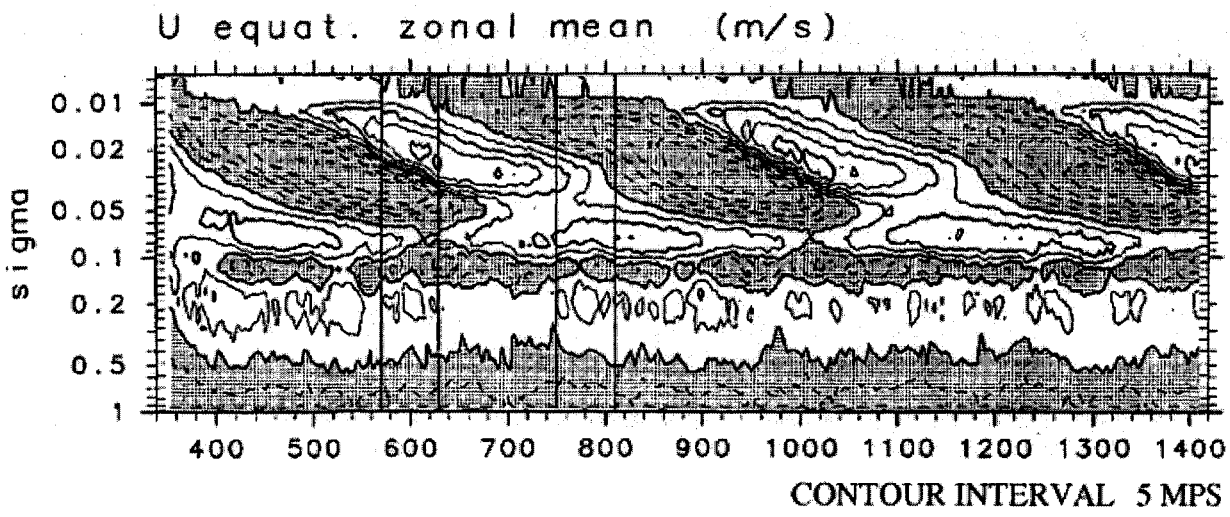

FROM HORINOUCHI AND YODEN, JAS, 55, 502 (1998)

Low-frequency waves

The effects of convective parameterizations are evident even in the troposphere. The following figures show:

- Power spectra of heating derived from OLR data and from model runs with both NCAR CCM3 convective parameterizations. Even at frequencies typical of the tropospheric Madden-Julian Oscillation (MJO) the Hack parameterization excites waves more efficiently than the Zhang-McFarlane parameterization

- Hovmoller diagram showing the MJO in CCM3 run with the Hack and Zhang-McFarlane parameterizations

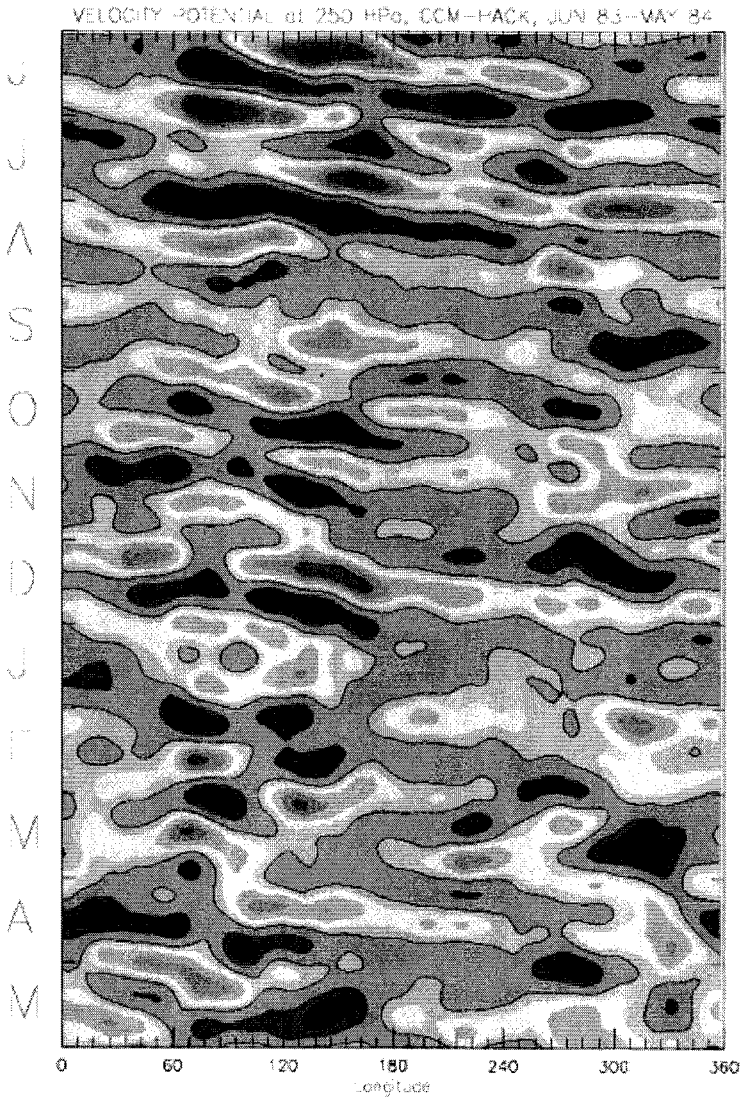
VELOCITY POTENTIAL at 250 HPa, CCM-PACK, JUN 83-MAY 84
J
J
A
S
O
N
D
J
F
M
A
M
0
60
120
180
240
300
360
Longitude
10N-10S average
20-100 days filter

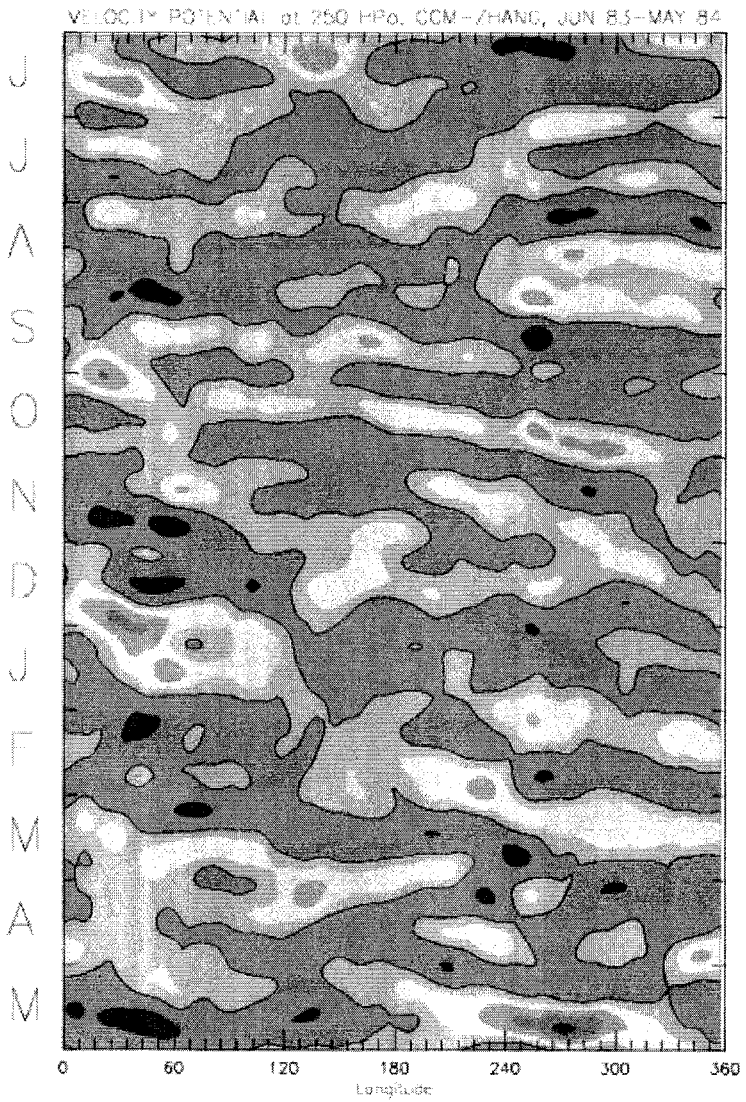
VELOCITY POTENTIAL at 250 HPa, CCM-/HANC, JUN 83-MAY 84
J
J
A
S
O
N
D
J
F
M
A
M
0
60
120
180
240
300
360
Longitude
10N-10S average
20-100 days filter

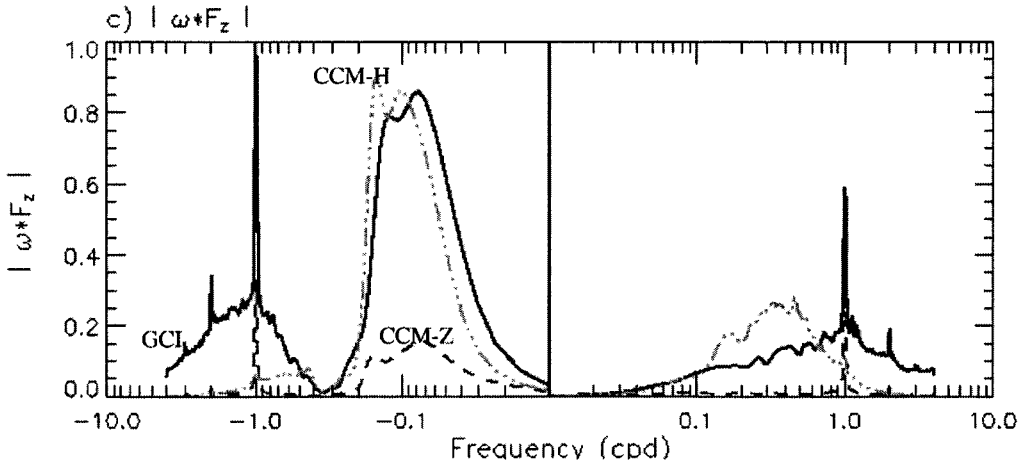

MJO: 0.016-0.033 cpd (30-60 days)

CONCLUSIONS

- Parameterizations produce widely different convective variability in GCMs, e.g.:
  - CCM3/Zhang-McFarlane: Very little variance at all frequencies
  - CCM3/Hack: Variance at low frequencies comparable to observations; much less than observed at higher frequencies
  - AGCM: Comparable to GCI observations over a wide range of frequency
- These differences have profound impacts on model tropical dynamics:
  - SAO and QBO
  - MJO
- Systematic analysis of convective parameterizations may be required to improve transient behavior, especially at high frequencies
- Work is also needed to determine more reliably the spectrum of convective variability from global OLR observations

BIBLIOGRAPHY

Baldwin, M.P., et al., 2001: The quasi-biennial oscillation. *Rev. Geophys.*, **39**, 179-229.

Bergman, J.W., and M.L. Salby, 1994: Equatorial wave activity from fluctuations in observed convection. *J. Atmos. Sci.*, **51**, 3791-3806.

Ebert, E.E., M.J. Manton, P.A. Arkin, R.J. Allam, G.E. Holpin and A. Gruber, 1996: Results from the GPCP Algorithm Intercomparison Programme. *Bull. Amer. Meteor. Soc.*, **77**, 2875-2887.

Ebert, E.E. and M.J. Manton, 1998: Performance of satellite rainfall estimation algorithms during TOGA COARE. *J. Atmos. Sci.*, **55**, 1537-1557.

Hendon, H.H. and K. Woodberry, 1993: The diurnal cycle of Tropical convection. *J. Geophys. Res*, **98**, 16623-16637.

Ricciardulli, L. and R.R. Garcia, 2000: The excitation of equatorial waves by deep convection in the NCAR Community Climate Model (CCM3). *J. Atmos. Sci.*, **57**, 3461-3487.

Salby, M.L. and R.R. Garcia, 1987: Transient response to localized episodic heating in the Tropics. Part I: Excitation and short-time near-field behavior. *J. Atmos. Sci.*, **44**, 458-498.

Salby, M.L., H.H. Hendon, K. Woodberry and K. Tanaka, 1991: Analysis of global cloud imagery from multiple satellites. *Bull. Amer. Meteor. Soc.*, **72**, 467-480.

Schiffer, R.A. and W.B. Rossow, 1983: The International Satellite Cloud Climatology Project (ISCCP): the first project of the World Climate Research Program. *Bull. Amer. Meteor. Soc.*, **64**, 779-784.

Tanaka, K.H., K. Woodberry, H.H. Hendon and M.L. Salby, 1991: Assimilation of global cloud imagery from multiple satellites. *J. Atmos. Ocean. Tech.*, **8**, 613-626.

Tiedke, M., 1989: A comprehensive mass flux scheme for cumulus parameterization in large-scale models. *Mon. Weather Rev.*, **117**, 1779-1800.